Journal of Catalysis 383 (2020) 60–76

Contents lists available at ScienceDirect

Journal of Catalysis

journal homepage: www.elsevier.com/locate/jcat

# Elementary steps and site requirements in formic acid dehydration reactions on anatase and rutile $TiO_2$ surfaces

Stephanie Kwon, Ting Chun Lin, Enrique Iglesia *

*Department of Chemical Engineering, University of California, Berkeley, CA 94720, United States*

ARTICLE INFO

*Article history:*
Received 30 July 2019
Revised 6 December 2019
Accepted 27 December 2019

*Keywords:*
$TiO_2$
Dehydration
Formic acid
Carboxylic acids
Acid-base pairs
Density functional theory

ABSTRACT

Mechanistic details of HCOOH decomposition routes provide valuable insights into reactions involving bound formates as intermediates or spectators; these routes are also widely used as a probe of the acid-base properties of oxide surfaces. The identity and kinetic relevance of bound intermediates, transition states, and elementary steps are reported here for HCOOH dehydration on anatase and rutile $TiO_2$ surfaces through complementary kinetic, isotopic, spectroscopic and theoretical assessments. Five-coordinate exposed $Ti_{5c}$ centers are saturated with bidentate formates ($^*HCOO^*$) at catalytic conditions (423–463 K; 0.1–3 kPa HCOOH), as evident from infrared spectra collected during catalysis and the amounts of HCOOH and CO evolved upon heating the $TiO_2$ samples containing pre-adsorbed HCOOH-derived species. These $^*HCOO^*$ species are inactive but form a stable "surface template" that contains stoichiometric protons onto which HCOOH binds molecularly (HCOOH-$H^*$) to form a coexisting adlayer. $H_2O$ elimination from HCOOH-$H^*$ is the sole kinetically-relevant step. DFT-derived barriers show that this step involves its reaction with $Ti_{5c}$-$O_{2c}$ that acts as a Lewis acid-base pair. Such route, in turn, requires the access of HCOOH-$H^*$ to a $Ti_{5c}$ center, which is made available through a momentary reprotonation of a $^*HCOO^*$. This step is much less facile on rutile than on anatase due to stronger acid strength of its $Ti_{5c}$ centers that binds $^*HCOO^*$ species more strongly and its shorter $Ti_{5c}$-$Ti_{5c}$ distances that induce greater repulsions between co-adsorbed $HCOOH^*$ formed upon reprotonation step. These differences account for low dehydration reactivity of rutile at these temperatures. This mechanistic interpretation is in full accord with DFT-derived barriers, binding energies, and kinetic isotope effects that quantitatively agree with the values from regressed kinetic and thermodynamic parameters, with *in-situ* infrared spectra that identify HCOOH-$H^*$ species as the sole reactive intermediates, and with the differences in turnover rates between anatase and rutile catalysts. These dehydration routes are also consistent with the surface chemistry expected for Lewis acid-base pairs on stoichiometry $TiO_2$ surfaces without requiring the presence or involvement of reduced centers or titanols in the catalytic cycle. The reaction routes described in this work show how strongly-bound species, evident in presence and unreactive nature from *in-situ* infrared spectra, provide an organic "permanent" template for reactions of weakly-bound species that are often invisible in spectroscopy.

## 1. Introduction

Formic acid (HCOOH) decomposition routes on metal oxides provide important insights into catalytic reactions that involve bound formates as intermediates, such as water–gas shift (WGS) [1] and methanol synthesis [2], for which oxides act as co-catalysts or promoters along with the requisite metal function [3,4]. These catalytic systems include metals (e.g. Cu, Pt, Au) that catalyze HCOOH dehydrogenation [5–7], but at rates inhibited by the CO co-reactant in such reactions, and oxides that catalyze HCOOH dehydration to CO and $H_2O$ [8–10]. Such site requirements implicate the plausible involvement of HCOOH as a molecular shuttle or a formate precursor in catalytic reactions involving CO, $H_2O$, $H_2$ or $CO_2$ reactants, specifically when the metal and oxide functions are separated by distances beyond atomic or molecular dimensions.

Here, HCOOH dehydration routes are examined at relevant WGS temperatures (423–463 K; 0.1–3 kPa HCOOH) on anatase and rutile $TiO_2$ powders ($TiO_2$(a), $TiO_2$(r)), which are known to promote WGS reactivities of the metal function (Pt, Au) [3,4] in order to assess the properties of oxide surfaces that govern their dehydration-hydration reactivities. The mechanistic details of

---

* Corresponding author.
*E-mail address:* iglesia@berkeley.edu (E. Iglesia).

https://doi.org/10.1016/j.jcat.2019.12.043
0021-9517/

HCOOH dehydration on $TiO_2$(a) and $TiO_2$(r) surfaces, including HCOOH binding modes and the nature of active centers, have remained controversial [11–16]. These oxides preferentially expose $TiO_2$(a)(1 0 1) and $TiO_2$(r)(1 1 0) facets that consist of Ti centers with five-fold ($Ti_{5c}$) and six-fold ($Ti_{6c}$) coordination linked through exposed O-atoms in either two-fold ($O_{2c}$) or three-fold ($O_{3c}$) coordination (Fig. 1) [17]. Scanning tunneling microscopy (STM) [18] and density functional theory (DFT) [19,20] indicate that HCOOH dissociates on $TiO_2$(r)(1 1 0) surface to form bidentate formate (*HCOO*) that interacts with two $Ti_{5c}$ centers and a proton added at an $O_{2c}$ center, saturating the surface with ordered structures at 1/2 monolayer (ML) coverage. However, the corresponding HCOOH adsorption modes on $TiO_2$(a)(1 0 1) are less certain. DFT methods indicate that HCOOH adsorbs molecularly (HCOOH*) via strong interactions with Lewis acid-base pairs consisting of exposed $Ti_{5c}$-$O_{2c}$ [21,22], but infrared (IR) spectra of HCOOH bound on $TiO_2$(a) powders show bands for both *HCOO* and HCOOH* species [23].

The relative surface coverages of HCOOH-derived species, their kinetic relevance during catalytic turnovers, and the active structures on $TiO_2$ surfaces that bind intermediates and transition states involved are also unclear. Surface defects are often implicated because they bind HCOOH-derived species strongly, thus allowing their adsorption and retention for studies that require low contacting pressure and high sticking probabilities. O-vacancies formed upon reduction of $Ti^{4+}$ centers to $Ti^{3+}$ were proposed as active centers for HCOOH dehydration on $TiO_2$(r)(1 1 0) based on STM images of $TiO_2$(r)(1 1 0) collected in contact with HCOOH ($1.33 \times 10^{-4}$ Pa s) and during successive thermal treatment at 350 K, combined with theoretical evidence [13,24]. Others, in contrast, support isolated titanols as the active structures in $TiO_2$(r) based on infrared spectra of $TiO_2$(r) samples in contact with $H_2O$ or HCOOH and the desorption and decomposition rates of pre-adsorbed $H_2O$ and HCOOH-derived species during temperature ramp (TPD) [9]. These previous studies, however, did not bring together kinetic, isotopic, spectroscopic and theoretical inquiries at conditions relevant for catalytic turnovers, an essential requirement for accurate mechanistic assessments, or establish differences in the identity and reactivity of the active sites on $TiO_2$(a) and $TiO_2$(r) surfaces.

This study reports the evidence gathered by combining these methods to address the enduring controversies about the mechanism and site requirements in HCOOH dehydration catalysis on $TiO_2$, a seemingly simple rearrangement relevant to other reactions (e.g., WGS, methanol synthesis, and photocatalytic HCOOH decomposition on $TiO_2$ [25]) and often employed as a model reaction to assess the nature and reactivity of metal and oxide catalysts [8,10]. The results of this study, in turn, show that HCOOH dehydration is catalyzed by $Ti_{5c}$-$O_{2c}$ pairs on stoichiometric surfaces of $TiO_2$(a) and $TiO_2$(r). These $Ti_{5c}$-$O_{2c}$ pairs contain $Ti_{5c}$ centers that are saturated with *HCOO* species at conditions of HCOOH dehydration catalysis (423–463 K; 0.1–3 kPa HCOOH). *HCOO* species are unreactive at these reaction temperatures but provide protons, onto which HCOOH adsorbs molecularly to form a co-existing adlayer. This $H^+$-bound molecular HCOOH (denoted as HCOOH-H*) eliminates $H_2O$ and acts as a sole intermediate. DFT-derived energies confirmed the presence and spectator nature of stable and unreactive *HCOO*-saturated surfaces and excluded several other plausible dehydration routes.

The proposed dehydration route involves HCOOH-$H^+$ reaction with a $Ti_{5c}$-$O_{2c}$ pair that is made available through a momentary re-protonation of a *HCOO* into a bound molecular HCOOH* interacting with a $Ti_{5c}$-$O_{2c}$ pair. This re-protonation step is much less facile on $TiO_2$(r) than on $TiO_2$(a) because (i) its $Ti_{5c}$ centers bind *HCOO* too strongly due to their stronger acid strengths (as shown by their more negative DFT-derived $OH^-$-binding energies [26]) and (ii) its shorter $Ti_{5c}$-$Ti_{5c}$ distances lead to the formation of less stable co-adsorbed HCOOH* species upon *HCOO* re-protonation and re-orientation of HCOOH-H* to a $Ti_{5c}$ center. Such difference in acid-base and structural properties accounts for a very low and nearly undetectable dehydration reactivity of $TiO_2$(r) at relevant conditions.

This mechanistic interpretation agrees well with all experimental observation and with DFT-derived energies and kinetic isotope effects that accurately capture measured values. These results, in turn, illustrate how strongly-bound species, evident in presence and unreactive nature from *in-situ* infrared spectra, provide an organic "permanent" template for reactions of weakly-bound species, without the reactivity often ascribed to bidentate formates. These mechanistic conclusions also offer a sobering reminder about the risks in selecting seemingly simple reactions to infer the nature and reactivity of active sites, unless accompanied by independent assessments of the number and type of binding sites and the identity, coverage and kinetic involvement of bound species (that are often weakly-bound and spectroscopically undetectable) and by the unequivocal elucidation of the identity and kinetic relevance of the elementary steps involved. It is our intent to also show through the approach and evidence reported here how diverse experimental tools and theoretical methods are required for definitive mechanistic conclusions and how these methods must accept and rigorously consider the crowded nature of surfaces during practical catalysis.

## 2. Methods

### 2.1. Experimental methods

#### 2.1.1. Catalyst preparation and characterization

$TiO_2$(a) (Sigma-Aldrich; 99.7%; 55 $m^2\ g^{-1}$) and $TiO_2$(r) (Sigma-Aldrich; 99.5%; 33 $m^2\ g^{-1}$) crystalline powders were pressed into pellets, crushed, and sieved to obtain aggregates (125–180 μm in diameter). These $TiO_2$ samples were treated at 723 K in flowing dry air (1.67 $cm^3\ s^{-1}$; 99.999%; Praxair) for 15 h before steady-state reaction and infrared experiments.

The phase purity and crystallinity of $TiO_2$ samples were confirmed using X-ray diffraction (XRD) before and after thermal

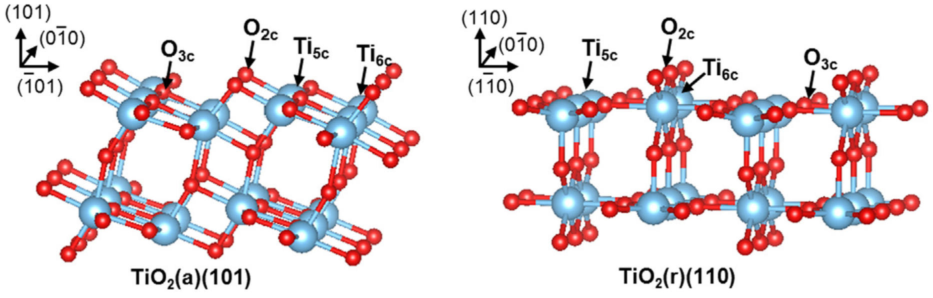

**Fig. 1.** DFT-derived structures for $TiO_2$(a)(1 0 1) and $TiO_2$(r)(1 1 0) surfaces.

treatments (Figs. S1 and S2 for $TiO_2$(a) and $TiO_2$(r), respectively; Supporting Information (SI)). The rutile contents in the $TiO_2$(a) samples were quantitatively assessed from measured X-ray diffractograms using direct comparison method [4,5], which relates the ratio of integrated intensities of the two phases to their volume fraction ratio. The surface areas of $TiO_2$ samples were determined from volumetric $N_2$ uptake data using BET analysis formalisms [27], which are used with crystallographic $Ti_{5c}$-$O_{2c}$ site densities of $TiO_2$(a)(1 0 1) and $TiO_2$(r)(1 1 0) surfaces (5.2 $nm^{-2}$) to estimate the number of $Ti_{5c}$-$O_{2c}$ pairs in order to report turnover rates (calculation details in SI; Section S.2).

### 2.1.2. Catalytic rate measurements

HCOOH dehydration rates were measured on $TiO_2$ samples (0.01–0.1 g) held within a U-shaped quartz tube (4 mm i.d.). The catalyst bed was diluted with acid-washed quartz powders in order to maintain plug-flow hydrodynamics and to avoid any temperature gradients; the quartz powders do not decompose HCOOH at any detectable rate at the conditions of catalytic measurements. Temperatures were measured using a thermocouple (K-type, Omega) placed within a dimple in the quartz tube at the location of the catalyst bed and maintained using a resistively-heated furnace with an electronic controller (Watlow, Series 982). HCOOH (Fisher Scientific; ≥98%) was introduced into a He stream (Praxair; 99.999%) at 323 K using a syringe pump (Cole Parmer, 74,900 series). $H_2O$ (doubly-distilled, deionized to ≥17.6 mΩ-cm) was introduced at 373 K through a separate port and transfer-lines using a syringe pump (Cole Parmer, 74,900 series) and mixed with the HCOOH reactants at the reactor inlet. All transfer lines except near the injection ports were kept at room temperature in order to prevent parasitic decomposition of HCOOH. Correspondingly, HCOOH and $H_2O$ pressures (<3 and <1.5 kPa, respectively) were kept well below their vapor pressures at 298 K (5.3 kPa and 3.2 kPa, respectively [28,29]). He (Praxair; 99.999%), CO (Praxair; 90% balance in Ar), $O_2$ (Praxair; dry air; 99.999%), and $H_2$ (Praxair; 99.95%) gases were metered by electronic mass flow controllers (Porter, Model 201) to set the intended concentrations in flowing streams. The identity and concentration of all species in the inlet and outlet streams were determined using on-line gas chromatography (Agilent, 6890A) equipped with a packed column (Agilent Porapak-Q, 4.8 m, 80–100 mesh) and a thermal conductivity detector (TCD). The retention time and response factors for all species were determined by using gases of known concentrations. Rates were also measured for HCOOD, DCOOH, and DCOOD (Cambridge Isotope Laboratories; ≥ 98% chemical and isotopic purities for each reagent) using the same procedure. Their isotopic purities during dehydration catalysis were confirmed with an on-line mass-spectroscopy (MKS Spectra, MiniLab LM80) that is used in parallel with gas chromatography.

In these experiments, the catalyst loadings and the flow rates of reactants are chosen to achieve differential conversions (<20%) at each condition; yet, the concentrations of HCOOH reactants and $H_2O$ products that inhibit the turnover rates change along the catalyst bed. In order to accurately account for such concentration gradients of reactants and products within the catalyst bed, the rate parameters were determined by regressing the measured rates to the integral form of the rate expression with ideal plug flow approximations (regression details in SI; Section S.2). These regressed parameters were then used to extrapolate the rates at zero residence time; these rates exclude any kinetic effect of $H_2O$ products formed during the reaction and are reported in Sections 3.1 and 3.5.

### 2.1.3. Infrared spectroscopy

Infrared spectra were collected in a transmission mode using a spectrometer (ThermoNicolet; Nexus 670), equipped with a Hg-Cd-Te (MCT) detector. Thin $TiO_2$ wafers (~10 mg $cm^{-2}$) were placed between KBr windows in a quartz *in-situ* cell. Temperatures were measured using a temperature input device (National Instruments, USB-TC01) with a thermocouple (K-type, Omega) placed at the outer edge of the wafer and controlled electronically (Watlow, Series 982) using resistive heating. All reagents and carrier gases were delivered to the system as described above and infrared spectra were collected at 2 $cm^{-1}$ resolution in the 4000–1000 $cm^{-1}$ wavenumber range by averaging 64 scans with the spectra of KBr wafers taken as background, unless stated otherwise.

These spectra were used to determine the presence of surface titanols and the identities, the kinetic relevance, and the surface coverages of bound HCOOH-derived species on $TiO_2$ surfaces. Titanols in $TiO_2$ samples were detected from infrared spectra collected during their thermal treatments (453–723 K) in flowing He, where the spectra were acquired during stepwise changes in temperature by holding for 0.5 h at each temperature. The identities of HCOOH-derived species bound at $TiO_2$ surfaces and their kinetic relevance were determined from infrared spectra collected during HCOOH dehydration reactions (1.5 kPa HCOOH; 433 K) and after the removal of HCOOH(g) from the He stream (433 K); prior to these measurements, the wafers were treated within the cell at 573 K for 0.5 h in flowing air (<0.05 ppm hydrocarbon; generated using Parker Balston HPZA-3500) in order to remove any surface-bound impurities before contact with reactants. The effect of HCOOH pressures on the surface coverages of these bound HCOOH-derived species was assessed from infrared spectra of $TiO_2$ samples in contact with HCOOH at various pressures (0.1–1.8 kPa HCOOH; 433 K); the wafers were cleaned between each measurement by thermally treating them at 573 K for 0.5 h in flowing air to remove any residual bound species. HCOOH dehydration rates were measured during these spectra acquisitions by analyzing the effluents from the infrared cell using a separate infrared gas analyzer (MKS, MultiGas Series 2000). The desorption and decomposition of bound HCOOH-derived species were examined from infrared spectra acquired upon heating the $TiO_2$ wafers after their exposure to HCOOH (0.5 kPa) at ambient temperature; for these measurements, spectra were obtained by averaging four scans in order to provide the temporal resolution required for analysis of the desorption and decomposition dynamics.

### 2.1.4. Temperature-programmed desorption and decomposition of HCOOH-derived adsorbed species

The number of bound HCOOH-derived species at $TiO_2$ surfaces were quantified by the detection of molecules evolved into a flowing He stream (1.5 $cm^3$ $s^{-1}$ $g^{-1}$) during the temperature ramp (ambient temperature to 673 K; 0.33 K $s^{-1}$) of $TiO_2$ powders (0.45–0.75 g) containing pre-adsorbed HCOOH-derived species. These bound HCOOH-derived species were formed by exposing $TiO_2$ powders, placed in the U-shaped quartz tube, to 0.5 kPa HCOOH (ambient temperature) until the composition of the effluent stream also reached at 0.5 kPa HCOOH. The speciation and quantification of the molecules evolved during the temperature ramp were carried out using an infrared analyzer (MKS, MultiGas Series 2000) with a 2.37 s temporal resolution. The reactor temperature was measured using a thermocouple (K-type, Omega) and logged using a temperature input device (National Instruments, USB-TC01). All reagents and carrier gases were delivered to the system as described above.

## 2.2. Density functional theory assessments of energies of bound intermediates and transition states, and elementary steps

DFT-derived energies and free energies of intermediates and transition states involved in HCOOH dehydration elementary steps were obtained using the Vienna ab-initio simulation package

(VASP) [30–32] with gradient-corrected Perdew–Burke–Ernzerhof (PBE) functionals [33] to describe the electron exchange and correlation. The core electrons were treated using projector-augmented wave (PAW) methods [34] with an energy cutoff of 396 eV. Grimme's D2 methods [35] were used to account for van der Waals (vdW) interactions that are essential to describe the weakly-bound surface species and adsorbate-adsorbate interactions prevalent at high surface coverages. Electronic energy optimization steps used convergence criteria of $1 \times 10^{-6}$ eV for energies and 0.05 eV $Å^{-1}$ for forces on all atoms. A Monkhorst–Pack grid of 8 × 8 × 8 was used for bulk calculations, while a 4 × 4 × 1 grid was used for all slab models.

The known structures of $TiO_2$(a) (tetragonal, $I4_1/amd$, a = b = 0.373, c = 0.937 nm) and $TiO_2$(r) (tetragonal, $P4_2/mnm$, a = b = 0.459, c = 0.295 nm) [17] were used as the starting point to determine DFT-derived lattice parameters for $TiO_2$(a) (a = b = 0.379, c = 0.952 nm) and $TiO_2$(r) (a = b = 0.457, c = 0.296 nm) that were similar to those reported from crystallographic data. The (1 0 1) and (1 1 0) surfaces, which represent the most exposed facets for $TiO_2$(a) [36] and $TiO_2$(r) [17], were used in all DFT calculations. The slab models of $TiO_2$(a)(1 0 1) and $TiO_2$(r)(1 1 0) surfaces were constructed from optimized bulk structures, each of which consisted of two Ti–O layers (Fig. 1); HCOOH binding energies differed by only 1 kJ $mol^{-1}$ for slab models with two or four Ti–O layers (Table S1; SI). The top $TiO_2$ layer and all bound species were fully relaxed in all calculations, while the bottom layer was held at the atomic positions present in bulk $TiO_2$. Supercells with 4 (1 × 2), 8 (2 × 2) and 16 (2 × 4) Ti–O pairs were used with one to eight HCOOH molecules per supercell in order to probe the effects of coverages on the energies of intermediates and transition states. Only $Ti_{5c}$-$O_{2c}$ pairs were examined and used to define fractional occupancies because coordinately-saturated $Ti_{6c}$ centers do not bind any intermediates or transition states, as shown by their nearly-zero DFT-derived $OH^-$(g) binding energy (−1 kJ $mol^{-1}$), in contrast with the value of −246 kJ $mol^{-1}$ at coordinately-unsaturated $Ti_{5c}$ centers in $TiO_2$(a)(1 0 1) [26]. Consequently, one HCOOH molecule on each 2 × 4 supercell represents 1/8 ML. The binding energies of bidentate formate (*HCOO*) at 1/2 ML calculated with two *HCOO* on 2 × 2 supercell and with four *HCOO* on 2 × 4 supercell were the same (−130 kJ $mol^{-1}$; DFT-derived electronic energy; Table S1; SI); thus, the 2 × 2 supercell with two bound *HCOO* was used to describe *HCOO*-saturated surfaces.

The minimum energy paths connecting the reactant and product states of each elementary step were calculated using nudge elastic band (NEB) methods [37] with the energy convergence criteria of $1 \times 10^{-4}$ eV and the force criteria of 0.3 eV $Å^{-1}$ for all atoms. The structures located at the maximum energy point along the reaction coordinate (derived from NEB calculations) were used as the initial guesses for a TS search using Henkelman's Dimer method [38] with the convergence criteria of $1 \times 10^{-6}$ eV for electronic energy and 0.05 eV $Å^{-1}$ for forces.

Enthalpies and free energies were calculated at reaction temperatures from DFT-derived electronic energies and vibrational frequencies in order to assess the kinetic relevance of specific elementary steps and to allow rigorous benchmarking of calculations against experiments. Vibrational frequencies for all optimized intermediates and TS structures were calculated using the VASP software; these frequencies were then used to estimate zero-point vibrational energies (ZPVE), as well as the vibrational contributions to entropies and enthalpies at each temperature using statistical mechanical formalisms [39]. The frequencies for the weak modes (<100 $cm^{-1}$) in weakly-bound species are inaccurate and often lead to incorrect entropy estimates [40]. These modes represent frustrated analogs of the translational and rotational modes of the corresponding species in the gas phases and contribute significantly to entropies. Here, the entropy contributions of these modes were thus replaced by a fraction (0.7) of the entropic components for gaseous molecules corresponding to such modes, as suggested previously from adsorption entropies of weakly-bound species on well-defined oxide surfaces [41]. These corrections for ZPVE, vibrational, translational, and rotational enthalpies and free energies were added to DFT-derived electronic energies to give enthalpies and free energies at each reaction temperature.

## 3. Results and discussions

### 3.1. Effects of reactant and product pressures for dehydration rates on anatase $TiO_2$

HCOOH dehydration turnover rates (per exposed $Ti_{5c}$-$O_{2c}$ pair) on $TiO_2$(a) are shown in Fig. 2a as a function of HCOOH pressure (0.1–3 kPa; 423–463 K). Rates increase monotonically with HCOOH pressure, first linearly and then more gradually above 1 kPa HCOOH, indicative of a Langmuir-type rate equation:

$$rate = \frac{\alpha P_{HCOOH}}{1 + \beta P_{HCOOH} + \gamma P_{H_2O}} \tag{1}$$

This dependence of rates on HCOOH pressure, in turn, suggests the involvement of HCOOH-derived species at coverages that approach saturation as HCOOH pressures increase, leading to rates that ultimately become independent of HCOOH pressure. The CO products formed in these reactions do not influence rates, even when added to the inlet stream at pressures above those prevalent during catalysis (0–1 kPa CO; 1.5 kPa HCOOH; 433 K; Fig. S3; SI). The $H_2O$ co-products, in contrast, inhibit the rates (0.1–1.5 kPa $H_2O$; 0.5 kPa HCOOH; 423–463 K; Fig. 2b) due to their competitive adsorptions with HCOOH(g) at the binding sites. This rate equation (Eq. (1)) describes all rate data accurately, as shown by the dashed curves in Fig. 2, which correspond to the functional form of Eq. (1) with regressed parameters. The elucidation of the chemical origins of these rate parameters requires information from isotopic, spectroscopic, and theoretical methods, as discussed in detail in the sections that follow.

The $\alpha$ parameter in Eq. (1) reflects the free energy of the kinetically-relevant transition state (TS) relative to a gas-phase HCOOH molecule. The involvement of the C–H or O–H bonds in HCOOH in the step mediated by this TS can be determined from the dehydration rates of HCOOH and of its isotopomers with C–D or O–D bonds. Dehydration turnover rates for HCOOD were only slightly lower (by factor of 1.6) than that for HCOOH, while the rates for DCOOH and DCOOD were similar to each other and about three-fold smaller than that for HCOOH (433 K; Fig. 3). These kinetic isotope effects (KIE) indicate that the kinetically-relevant TS involves the partial cleavage of the C–H bond but not the O–H bond. The $\beta$ parameter in Eq. (1) reflects the free energy change of forming HCOOH-derived bound species from HCOOH(g), the species that saturate the active sites as the HCOOH pressure increases. The identities of such HCOOH-derived species and their relative coverages are discussed next in the context of infrared spectra measured during dehydration catalysis and during the decomposition of pre-adsorbed HCOOH-derived species upon temperature ramping.

### 3.2. Infrared assessments of the identity, coverage, and kinetic relevance of HCOOH-derived species on anatase $TiO_2$

Fig. 4a shows infrared spectra (in the range of 1000–2100 $cm^{-1}$) of the $TiO_2$(a) sample collected during steady-state HCOOH dehydration at 433 K (1.5 kPa HCOOH) and after the removal of

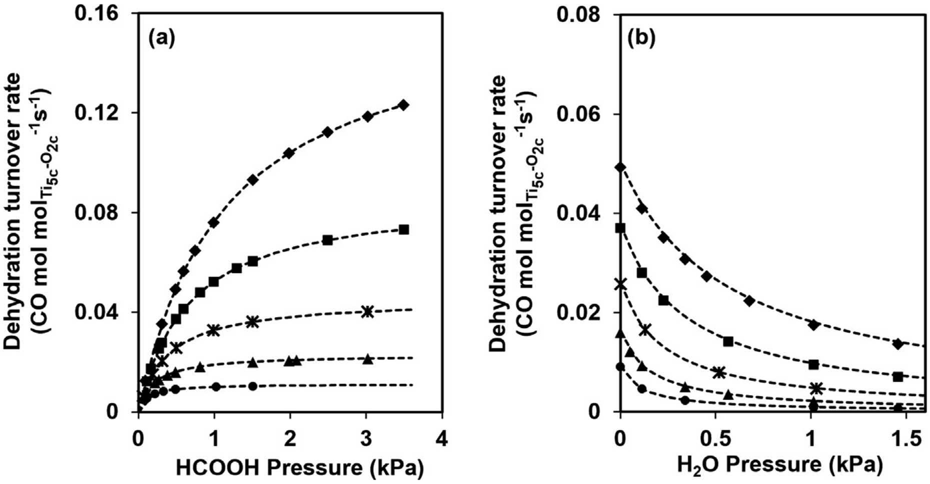

**Fig. 2.** HCOOH dehydration turnover rates measured on $TiO_2$(a) at 423 K (●), 433 K (▲), 443 K (*), 453 K (■), and 463 K (◆) as a function of (a) HCOOH pressure (0.1–3 kPa) and (b) $H_2O$ pressure (0.1–1.5 kPa; 0.5 kPa HCOOH). Reported rates were extrapolated to zero conversion using the integral form of Eq. (1) with ideal plug flow approximations. Dashed curves represent the best regression fits of the rates to the functional form of Eq. (1).

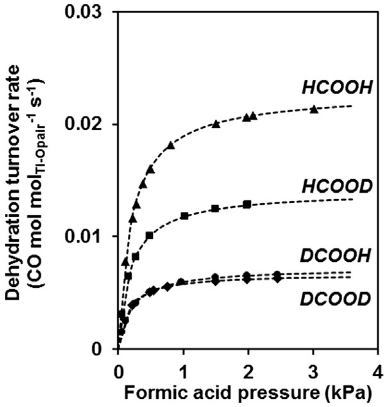

**Fig. 3.** Dehydration turnover rates of HCOOH (▲), HCOOD (■), DCOOH (●), and DCOOD (◆) on $TiO_2$(a) at 433 K as a function of formic acid pressure (0.1–3 kPa).

HCOOH(g) from the flowing He stream; these reflect the differential spectra, obtained by subtracting the spectrum of the $TiO_2$(a) sample measured at 433 K in flowing He after its treatment in $O_2$ (20 kPa; 573 K; 0.5 h). The bands for HCOOH(g) (1792, 1757, 1370, 1218, 1120, and 1088 cm$^{-1}$; Table 1) disappear immediately upon its removal from the inlet stream, while the bands at 1554 and 1359 cm$^{-1}$ persist even 1.5 ks after HCOOH(g) removal. These latter bands reflect antisymmetric and symmetric COO stretches for bidentate formate (*HCOO*) bound at two $Ti_{5c}$ centers [22,23], consistent with DFT-derived frequencies (1519 and 1339 cm$^{-1}$; Table 1). The estimated time required to convert 90% of the surface-bound intermediates to CO products at 433 K is 0.1 ks, assuming the first-order decomposition, taken together with the zero-order CO formation rate measured at 433 K (0.02 s$^{-1}$; Fig. 2a; calculation details in Section S.3.; SI). The bands associated with *HCOO* (1554 and 1359 cm$^{-1}$), however, remain even after 1.5 ks, indicative of the inactive nature of these strongly bound *HCOO* species during catalytic turnovers at 433 K.

The integrated intensity of distinct *HCOO* band at 1554 cm$^{-1}$ remains insensitive to HCOOH pressures as the pressure increases from 0.1 to 1.8 kPa (433 K; Fig. 4b). Such trend contrasts the observed effect of HCOOH pressure on dehydration turnover rates, which follow a Langmuirian behavior (Fig. 2a), and infers the involvement of a different type of bound species that vary in coverage over the range of HCOOH pressures, which leads to constant

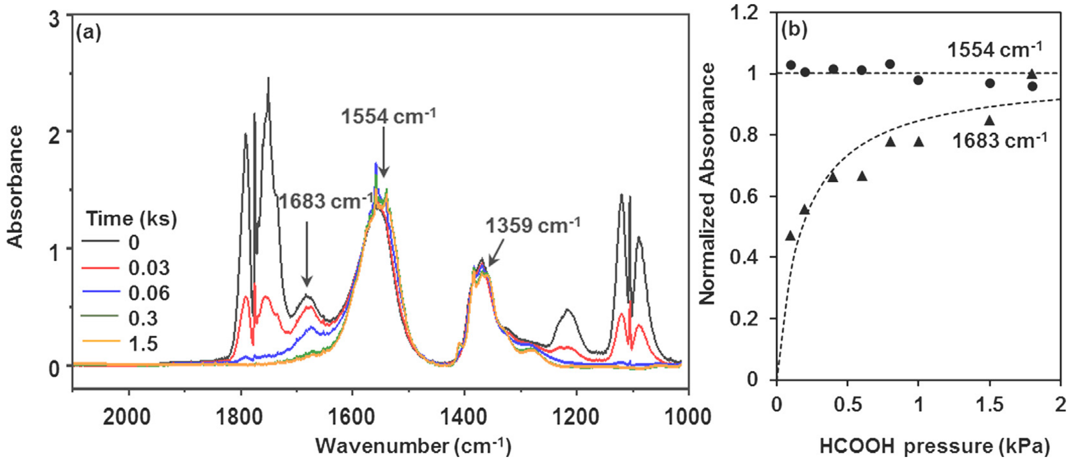

**Fig. 4.** (a) Infrared spectra of $TiO_2$(a) during steady-state HCOOH dehydration (1.5 kPa HCOOH; 433 K) and after the removal of HCOOH(g) from the reactant stream (0.03–1.5 ks). The spectrum of the $TiO_2$(a) sample measured at 433 K in flowing He after its treatment in $O_2$ (20 kPa; 573 K; 0.5 h) was taken as a reference. (b) The integrated absorbance for the bands at 1554 cm$^{-1}$ (for *HCOO*) (●) and at 1683 cm$^{-1}$ (for HCOOH-H*) (▲) as a function of HCOOH pressure (0.1–1.8 kPa; 433 K), normalized by their maximum values at the highest HCOOH pressure (1.8 kPa) used in these experiments.

**Table 1**
Vibrational frequencies ($cm^{-1}$) derived from infrared measurments on $TiO_2$(a) (1.5 kPa HCOOH; 433 K; spectra shown in Fig. 4a) and from DFT methods.

| | | (O–H) stretching | (C–H) stretching | (C=O) stretching | (C–H) bending | (O–H) bending | (C–O) stretching |
|---|---|---|---|---|---|---|---|
| HCOOH(g) | Exp. | 3591, 3541 | 3103, 3008 | 1792, 1757 | 1370 | 1218 | 1120, 1088 |
| | DFT | 3601 | 2971 | 1760 | 1347 | 1257 | 1077 |
| Molecular HCOOH | Exp. | | | 1683 | | | |
| | DFT (at $Ti_{5c}$)[a] | 2058 | 2997 | 1595 | 1365 | 1287 | 1119 |
| | DFT (at $H^+$)[b] | 3634 | 2965 | 1665 | 1360 | 1351 | 1218 |
| | | (O–H) stretching | (C–H) stretching | $(COO)_{as}$ stretching | (C–H) stretching | | $(COO)_s$ stretching |
| Bidentate formate | Exp. | | | 1554 | | | 1359 |
| | DFT[a] | 3661 | 2958 | 1519 | 1359 | | 1339 |
| Monodentate formate | DFT[a] | 3615 | 2888 | 1702 | 1330 | | 1136 |

[a,b] DFT calculations are performed at (a) 1/8 ML acid coverage and (b) 1/4 ML acid coverage on *HCOO*-saturated surfaces.

*HCOO* coverages. These data, in turn, show that *HCOO* species are not responsible for the β parameter in Eq. (1) and act as unreactive spectators at conditions of HCOOH dehydration catalysis (423–463 K; 0.1–3 kPa HCOOH).

Another distinct but weaker band is evident at 1683 $cm^{-1}$. This band becomes weaker and ultimately disappears after 0.06 ks upon the removal of HCOOH(g) from the reactant stream (Fig. 4a), consistent with the time required to decompose 90% of the surface-bound intermediates to form CO products at 433 K (0.1 ks; calculation details in Section S.3; SI). This 1683 $cm^{-1}$ band is previously assigned to a C=O stretching mode for molecular HCOOH bound at a $Ti_{5c}$ center via its C=O group (HCOOH*) [42]; the shift of the C=O stretching mode in HCOOH(g) at 1792 and 1757 to a lower wavenumber, 1683 $cm^{-1}$, supports the strong interaction of its C=O with the surface acid site. The observed frequency (1683 $cm^{-1}$), however, is much higher than the value expected from DFT methods (1595 $cm^{-1}$; Table 1). While this band may instead correspond to the antisymmetric COO stretching mode for monodentate formate at a $Ti_{5c}$ center (1702 $cm^{-1}$; Table 1), DFT-derived free energy change for monodentate formate formation from HCOOH(g) is much less negative than that for HCOOH* ($\Delta G_{ads}$ = −11 vs. −47 kJ $mol^{-1}$; 1/8 ML; 433 K), suggesting that the 1683 $cm^{-1}$ band is also unlikely to arise from monodentate formate. The coexistence of bidentate formate (*HCOO*) with those leading to the 1683 $cm^{-1}$ band suggests that this band may instead correspond to HCOOH adsorbed molecularly via interactions of its C=O with the proton (HCOOH-H*) formed at the surface $O_{2c}$-atom upon *HCOO* formation from HCOOH(g). Consistently, DFT-derived frequency for C=O stretching of HCOOH-H* species (1665 $cm^{-1}$; Table 1) is closer to the observed band (1683 $cm^{-1}$; Fig. 4a) than the frequency corresponding to HCOOH* at a $Ti_{5c}$ center (1595 $cm^{-1}$; Table 1).

The full range of infrared spectra (1000–4000 $cm^{-1}$) measured at 433 K on $TiO_2$(a) in contact with 1.5 kPa HCOOH and after removal of HCOOH(g) from He stream are shown in Fig. S4a (SI), along with the enlarged infrared spectra in the range of OH region (4000–3000 $cm^{-1}$) (Fig. S4b; SI). Upon the removal of HCOOH(g) from the reactant stream, infrared bands at 3550 and 3589 $cm^{-1}$ associated with HCOOH(g) disappear, while the new band at 3655 $cm^{-1}$ emerges. This weak band reflects the presence of OH groups, as expected from the formation of protons upon dissociative HCOOH adsorption to form bidentate formates at 433 K. This band at 3655 $cm^{-1}$ is very weak and becomes undetectable upon introduction of 1.5 kPa HCOOH(g); concurrently, a new broad feature at 3000–3500 $cm^{-1}$ appears, reflecting the H-bonding of these OH groups with HCOOH(g) that leads to the broadening of the band and a shift to lower frequencies [43]. These results, in turn, support the addition of protons at surface O-atoms upon dissociative HCOOH adsorption, and their interactions with HCOOH. The weak nature of this O–H band, however, imposes difficulties in drawing quantitative conclusion; this band becomes undetectable even at the lowest HCOOH pressure (0.1 kPa) employed in the experiment. As a result, more evident infrared band at 1683 $cm^{-1}$ was monitored to assess the effect of HCOOH pressure on surface coverage of HCOOH-H*.

The intensity of 1683 $cm^{-1}$ band initially increases linearly with HCOOH pressure and then more gradually at higher pressures (>1 kPa HCOOH), as shown by its integrated intensity (normalized by that at 1.8 kPa; 0.1–1.8 kPa HCOOH; 433 K; Fig. 4b). This normalized infrared absorbance reflects the fractional coverage of HCOOH-H* species during dehydration catalysis, which can be accurately described by the Langmuirian adsorption equation:

$$\theta_{HCOOH-H*} = \frac{K_1 P_{HCOOH}}{1 + K_1 P_{HCOOH}}, \quad (2)$$

evident from the dashed curve in Fig. 4b. The $K_1$ value obtained by regressing the data in Fig. 4b to the functional form of Eq. (2) (5 ± 2 $kPa^{-1}$; 433 K) is very similar to the value for the $\beta$ parameter (Eq. (1)) regressed from rate data (4.8 ± 0.4 $kPa^{-1}$; 433 K; Fig. 2). Such quantitative agreement, in turn, infers HCOOH-H* species as the most abundant surface intermediates (MASI) involved in HCOOH dehydration events, which saturate the surface and result in constant turnover rates at high HCOOH pressures (Fig. 2a).

The involvement of proton-bound HCOOH-H* intermediates in dehydration catalysis has been previously suggested for $Al_2O_3$, evidenced by titrating such protons with pyridine before and after the introduction of HCOOH to the reactant stream [44]. This work also showed that Lewis acid sites originally retained in the $Al_2O_3$ samples, in fact, are essentially destroyed upon introduction of HCOOH above 323 K. If this is also the case for $TiO_2$, this may suggest the presence of inactive *HCOO* species at their maximum 0.5 ML coverage, saturating all Lewis acid $Ti_{5c}$ centers on $TiO_2$ surfaces during dehydration catalysis. Such quantitative assessment of *HCOO* species is discussed in the next section by counting the number of HCOOH and CO molecules evolved upon heating $TiO_2$(a) powders containing pre-adsorbed HCOOH-derived bound species (TPD/TPSR).

### *3.3. Identities and surface coverages of bound species formed upon contact of anatase $TiO_2$ surfaces with HCOOH*

The exposure of $TiO_2$(a) powders to HCOOH (0.5 kPa) at ambient temperature leads to the evolution of HCOOH, CO, and $H_2O$ during subsequent temperature ramping. The amounts desorbed correspond to a surface stoichiometry (defined as the number of HCOOH per $Ti_{5c}$-$O_{2c}$ site pair) of near unity (0.99), estimated by integrating HCOOH and CO evolution rates (in Fig. S5a; SI) over time. The bound species detected by infrared spectroscopy upon contact with 0.5 kPa HCOOH at ambient temperature are bidentate formate (*HCOO*) and molecular HCOOH bound at protons (HCOOH-H*) (spectra at 300 K in Fig. S6a; SI). During the temperature ramping, the intensity of the *HCOO* band at 1554 $cm^{-1}$ decreased only at temperature above 473 K (Fig. 5a), indicative of its unreactive nature during catalytic turnovers at 423–463 K.

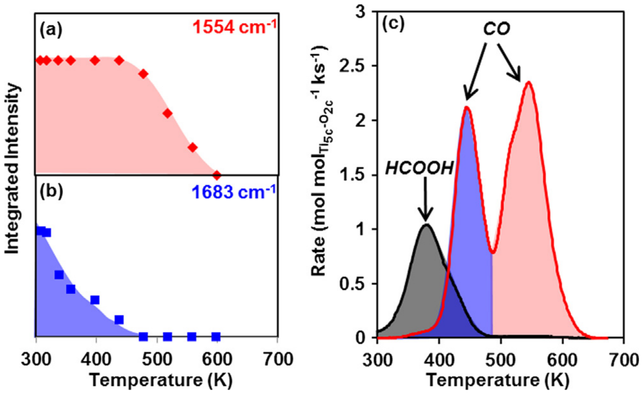

**Fig. 5.** The integrated absorbance for the infrared bands at (a) 1554 cm$^{-1}$ (for *HCOO*) and (b) 1683 cm$^{-1}$ (for HCOOH-H*) and (c) the HCOOH and CO evolution rates as a function of temperature (300–700 K) measured upon heating (in flowing He) the $TiO_2$(a) sample containing pre-adsorbed HCOOH-derived species.

Above 473 K, these *HCOO* species recombine with protons present at vicinal $O_{2c}$ centers to form CO(g) and $H_2O$(g) (Fig. 5c). The band for HCOOH-H* (at 1683 cm$^{-1}$), in contrast, decreased monotonically as temperature increased from 300 K and became undetectable above 473 K (Fig. 5b), as a consequence of the desorption of unreacted HCOOH and its dehydration products (Fig. 5c).

The different temperatures required for the desorption or reaction of *HCOO* and HCOOH-H* on $TiO_2$(a) surfaces allow the estimation for the number of bound species of each type. The disappearance of the 1683 cm$^{-1}$ band (for HCOOH-H*) at temperatures below those required for *HCOO* decomposition (above 473 K; Fig. 5a and 5b) indicates that the number of CO molecules evolved above 473 K corresponds to bound *HCOO* species (Fig. 5c). The deconvolution and integration of CO peaks in Fig. 5c give 0.46 CO per $Ti_{5c}$-$O_{2c}$ center (*HCOO*/$Ti_{5c}$-$O_{2c}$) = 0.46) from *HCOO* decomposition above 473 K, stoichiometrically consistent with the saturation of all $Ti_{5c}$ centers with *HCOO* species at the temperatures used here for HCOOH dehydration catalysis (423–463 K).

The full titration of each $Ti_{5c}$ center by unreactive *HCOO* species requires that molecular HCOOH species, present at HCOOH/($Ti_{5c}$-$O_{2c}$) ratios of 0.53 (from the CO and HCOOH evolved below 473 K; Fig. 5c), bind without their access to $Ti_{5c}$ centers. The measured adsorption stoichiometry of molecularly bound HCOOH species is consistent with their binding at the protons in the saturated bidentate template, which are present at a coverage of one $H^+$ per two $Ti_{5c}$ centers. This evidence from infrared and TPD/TPSR measurements led us to conclude that the active surfaces consist of *HCOO* species that present at their saturation 1/2 ML coverages and act as an unreactive organic template. Such *HCOO* template contains stoichiometric (1/2 ML) coadsorbed protons that act as the binding points for the reactive HCOOH-H* species. These proton-bound HCOOH-H* species are the sole reactive intermediates; their coverages change with HCOOH pressure in a manner consistent with the effects of pressure on dehydration turnover rates. Elimination of $H_2O$ from these HCOOH-H* intermediates may proceed by reacting with the proton, as previously suggested for $Al_2O_3$ catalyst [44], or with the Lewis acid $Ti_{5c}$ center that is preoccupied with *HCOO* at relevant conditions. DFT methods are used next to assess these two plausible reaction routes that are otherwise indistinguishable from experiments.

### 3.4. Theoretical treatments of HCOOH dehydration elementary steps, bound species and transition states on *HCOO*-saturated $TiO_2$(a)

The infrared and TPD/TPSR data in the previous sections provide experimental evidence for the permanence of a saturated *HCOO* template during HCOOH dehydration catalysis on $TiO_2$(a) (0.1–3 kPa HCOOH; 423–463 K). The stable and inactive nature of *HCOO* is consistent with the DFT-derived free energy change for its formation from HCOOH(g) on $TiO_2$(a)(1 0 1) that is large and negative ($\Delta G_{ads}$ = −57 kJ mol$^{-1}$; 433 K; 1/8 ML; 1 bar HCOOH; Table 2). This free energy change varies only from −57 to −54 kJ mol$^{-1}$, as *HCOO* coverage increases from 1/8 ML (no neighboring *HCOO*) to its saturated 1/2 ML coverage (Table 2), indicative of a very weak adsorbate–adsorbate repulsion within the *HCOO* template on $TiO_2$(a)(1 0 1).

DFT-derived free energy changes for the formation of monodentate formate and molecularly bound HCOOH at the $Ti_{5c}$ center (via either its C=O or O–H group) from HCOOH(g) are much less negative than that for bidentate formate at 1/8 ML coverage ($\Delta G_{ads}$ = −11, −47, −12 vs. −57 kJ mol$^{-1}$; 433 K; Fig. 6; Table 2), consistent

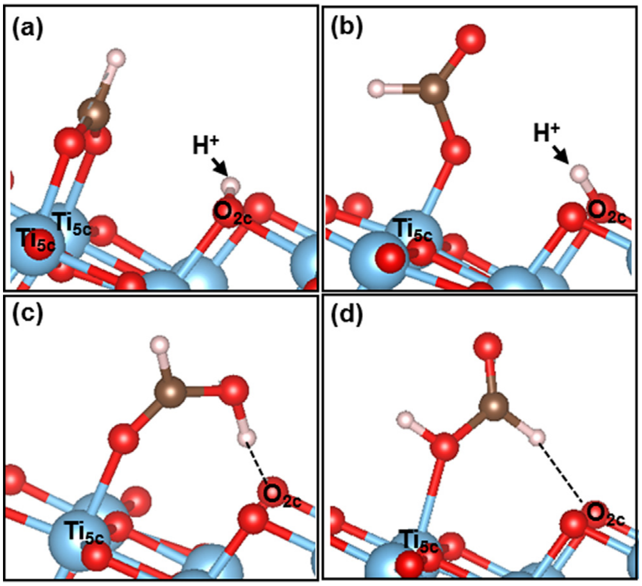

**Fig. 6.** DFT-derived HCOOH binding modes on $TiO_2$(a)(1 0 1): (a) bidentate formate, (b) monodentate formate, and (c) molecularly bound HCOOH at a $Ti_{5c}$ center (HCOOH*) via its C=O group and (d) via its O–H group.

**Table 2**

DFT-derived free energy change for the formation of bidentate and monodentate formates and molecularly bound HCOOH at a $Ti_{5c}$ center (HCOOH*) via its C=O or O–H groups from HCOOH(g) on the $TiO_2$(a)(1 0 1) surface[a].

| Adsorption mode | | Figure | Coverage (ML) | $\Delta G_{ads}$ (kJ mol$^{-1}$) |
|---|---|---|---|---|
| Bidentate formate | | 6a | 1/8 | −57 |
| | | | 1/2 | −54 |
| Monodentate formate | | 6b | 1/8 | −11 |
| HCOOH* | on $Ti_{5c}$ through C=O | 6c | 1/8 | −47 |
| | on $Ti_{5c}$ through O–H | 6d | 1/8 | −12 |

[a] Free energies are derived at 433 K and standard HCOOH pressure (1 bar).

with the predominant formation of *HCOO* upon HCOOH adsorption. Such conclusions contradict those in previous DFT studies, which concluded that $Ti_{5c}$-bound HCOOH* via its C=O group is the most stable bound structure on $TiO_2$(a)(1 0 1) [21,22], because vdW interactions were excluded from these calculations; DFT-derived adsorption energies for each binding modes calculated with (PBE-D2/PAW) and without vdW corrections (PBE/PAW) are compared in Table S2 (SI) with their comparisons to previously reported energies. These results, in turn, emphasize the importance of vdW corrections to DFT results in order to accuratly capture the preferred adsorption modes. Our DFT results with vdW corrections are in full agreement with experiments that provide clear evidence for the saturation of $Ti_{5c}$ centers with strongly bound *HCOO* (Sections 3.2 and 3.3).

HCOOH(g) binds at a proton (HCOOH-H*) that presents as a part of the saturated *HCOO* adlayer that constitutes the refractory organic template. This HCOOH-H*, the reactive intermediate, can undergo elimination reaction to form CO and $H_2O$ products via its reaction with a $H^+$-$O_{2c}$ pair or with a $Ti_{5c}$-$O_{2c}$ pair (Schemes 1 and 2). DFT-derived free energies (433 K; 1 bar HCOOH) of intermediates and transition states involved in these routes are shown in Fig. 7 with their structures shown in Figs. 8 and 9 for the routes involving $H^+$-$O_{2c}$ and $Ti_{5c}$-$O_{2c}$ pairs, respectively. All free energies are referenced to the reactant state of HCOOH(g) and *HCOO*-saturated template and reported at 1/4 ML HCOOH-H* coverage. These energies are expected to be similar at higher coverages as interactions among adsorbates are small, evidenced by HCOOH-H* formation energy from HCOOH(g) that varies by <2 kJ $mol^{-1}$ between 1/8 ML (isolated HCOOH-H*) and saturation coverages (1/2 ML) (Fig. S7; SI).

Whether HCOOH-H* eliminates $H_2O$ via its reactions with a $H^+$-$O_{2c}$ pair (Scheme 1) or a $Ti_{5c}$-$O_{2c}$ pair (Scheme 2), the first step involves its formation from HCOOH(g) via interactions of its O-atom in the C=O group with a proton in a *HCOO* template and its H-atom in the O–H group with the vicinal $O_{2c}$-atom (Figs. 8i and 9i) (step 1; Schemes 1 and 2). Such adsorption step is exoergic with the free energy change of −23 kJ $mol^{-1}$ (433 K; Fig. 7). In the case of reactions with a $H^+$-$O_{2c}$ pair (Scheme 1), this HCOOH-H* then undergoes intramolecular rearrangement to place its O-atom in the O–H group at the proton and its H-atom in the C–H group at a vicinal $O_{2c}$ center to create a configuration in which the $H^+$-$O_{2c}$ moiety acts as a Lewis acid-base pair (Fig. 8ii) (step 2; Scheme 1). This reorientation step is endoergic ($\Delta G$ = +36 kJ $mol^{-1}$; 433 K; Fig. 7); it appears along the reaction coordinate as a "ledge" to climb to the energy of the kinetically-relevant TS (Fig. 8iii). This TS contains the C–O bond in HCOOH-H* that is partially-cleaved as the CO molecule incipiently leaves upon the formation of $H_2O$ via the O-atom in the O–H group attacking the bound proton. The C–H bond is also partially-cleaved at this TS via H-abstraction by the surface $O_{2c}$-atom (step 3; Scheme 1). The weakly-bound CO formed in this step (Fig. 8iv) desorbs in an exoergic step ($\Delta G$ = −45 kJ $mol^{-1}$; 433 K; Fig. 7); the weak CO binding at the proton is consistent with negligible effect of CO pressure on dehydration turnover rates (Fig. S3; SI). More strongly-bound $H_2O$ at the proton (Fig. 8v) desorbs in the endoergic step ($\Delta G$ = +8 kJ $mol^{-1}$; 433 K; Fig. 7) to complete a HCOOH dehydration turnover (step 4; Scheme 1); this $H_2O$ adsorption and desorption step is quasi-equilibrated, evident from the effect of $H_2O$ that inhibits the rates (Fig. 2b). This dehydration route on a $H^+$-$O_{2c}$ pair forms CO and $H_2O$ without any disruptions of the strongly-bound bidentate formate template.

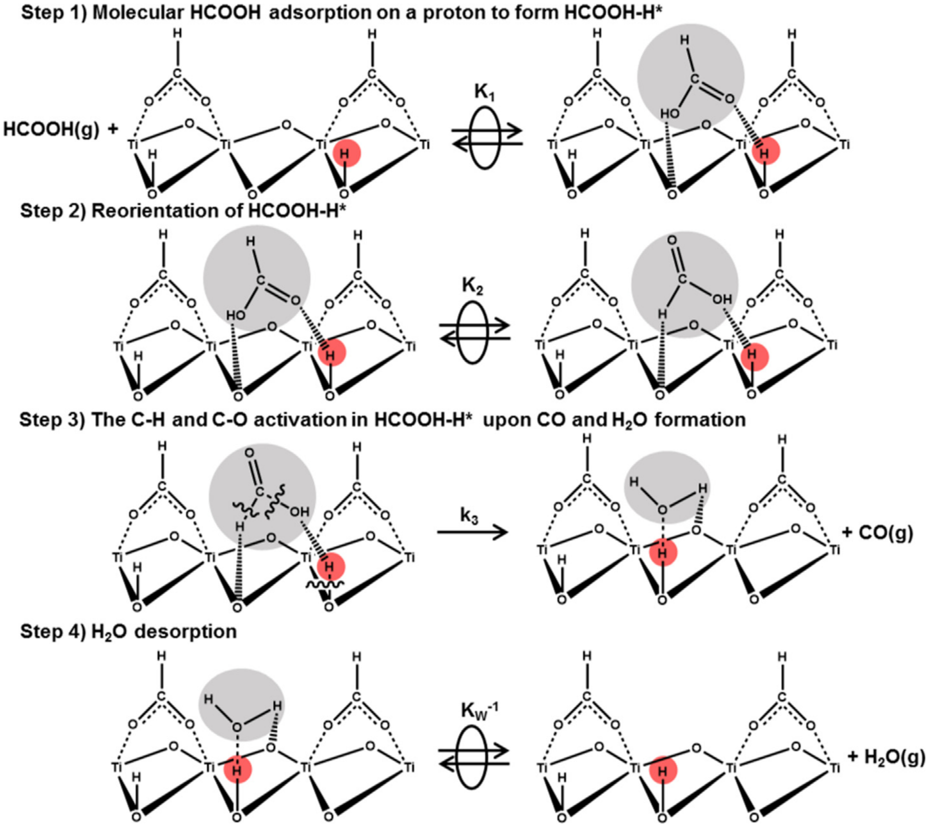

[a]Quasi-equilibrated steps are denoted by oval symbols placed over double arrows.

**Scheme 1.** HCOOH dehydration elementary steps via reactions with a $H^+$-$O_{2c}$ pair in a *HCOO* template.

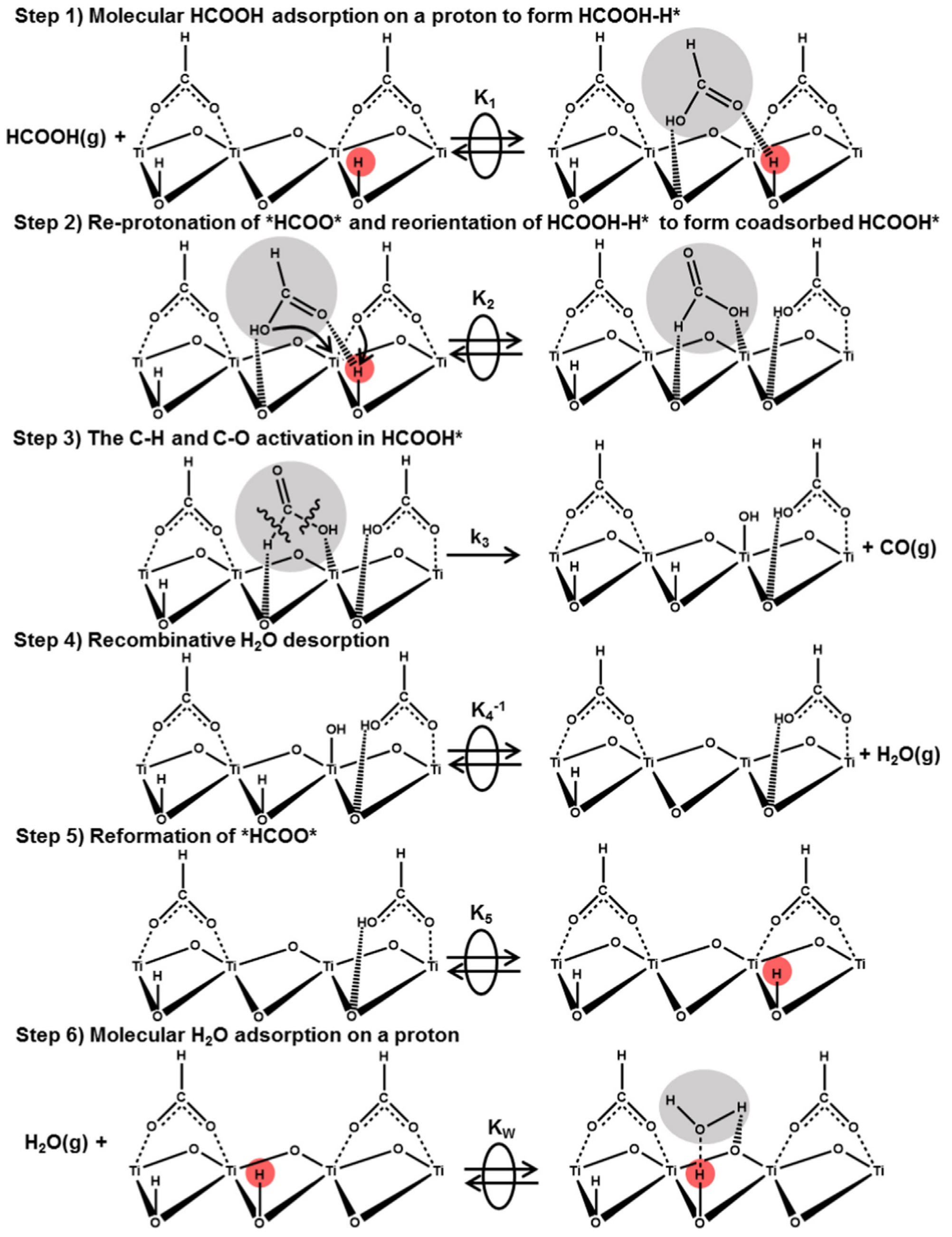

[a]Quasi-equilibrated steps are denoted by oval symbols placed over double arrows.

**Scheme 2.** HCOOH dehydration elementary steps via reactions with a $Ti_{5c}$-$O_{2c}$ pair in a *HCOO* template.

Another plausible route involves the reaction of HCOOH-H* with a $Ti_{5c}$-$O_{2c}$ pair (Scheme 2), which, in turn, requires its coordination to a $Ti_{5c}$ center that is already taken by *HCOO*. In order to do so, a *HCOO* next to HCOOH-H* is "shoved" and reprotonated to form a molecular HCOOH interacting with a $Ti_{5c}$ center (HCOOH*) via its O-atom in the C=O group and with a $O_{2c}$ center via its H-atom in the group O–H (Fig. 9ii) (step 2; Scheme 2). Such a "shoving" step is made energetically unfavorable by the need to cleave one of the two strong $Ti_{5c}$-O bonds in *HCOO* ($\Delta G$ = +8 kJ mol$^{-1}$; 433 K; Fig. 7) but is compensated in part by rearranging HCOOH-H* into a more stable molecular HCOOH that interacts with the $Ti_{5c}$ center (made available by detaching the O-atom in the "shoved" *HCOO*) via its O-atom in the O–H group and with the $O_{2c}$ center via its H-atom in the C–H group (Fig. 9ii). This HCOOH* formed upon reorientation of HCOOH-H* then cleaves its C–O bond to form a weakly-bound CO by attacking the acid $Ti_{5c}$ center via its O-atom in the O–H group and its C–H bond upon H-abstraction by the vicinal $O_{2c}$ center (Fig. 9iv) (step 3; Scheme 2). The TS mediating in this step imposes the highest barrier along the $H_2O$ elimination reaction coordinate and includes partially cleaved C–O and C–H bonds (Fig. 9iii). The weakly-bound CO formed desorbs in a subsequent exoergic step ($\Delta G$ = –33 kJ mol$^{-1}$; 433 K; Fig. 7). The resulting O–H group that remains at the $Ti_{5c}$ center and the H-atom at the $O_{2c}$ center (Fig. 9v) recombine to form a molecular $H_2O$ bound at the $Ti_{5c}$ center (Fig. 9vi); this step is exoergic with the free energy change of –15 kJ mol$^{-1}$ (433 K; Fig. 7). $H_2O$ desorbs in a subsequent endoergic step ($\Delta G_{des}$ = +38 kJ mol$^{-1}$; 433 K; Fig. 7) (step 4; Scheme 2). Finally, the "shoved" HCOOH* dissociates to reform *HCOO* in a slightly exoergic step (Fig. 9viii) ($\Delta G$ = –1 kJ mol$^{-1}$; 433 K; Fig. 7) (step 5; Scheme 2), thus

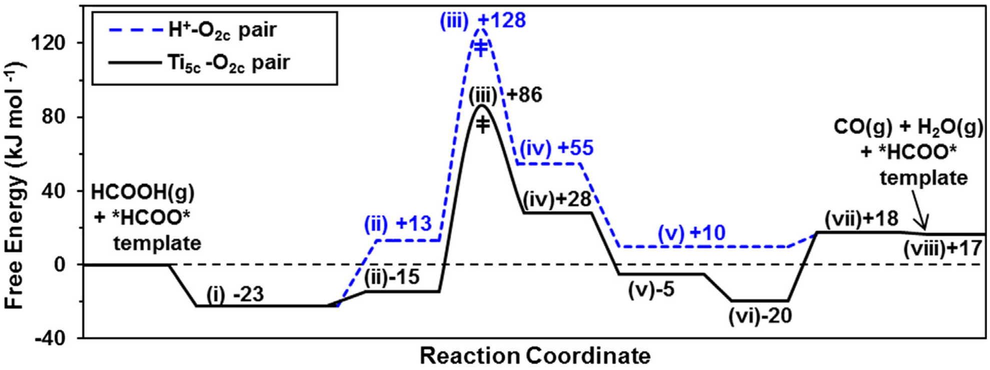

**Fig. 7.** DFT-derived free energies (kJ mol$^{-1}$; 433 K; 1 bar HCOOH) of intermediates and TS involved in HCOOH dehydration via reactions with a $H^+$-$O_{2c}$ pair (Scheme 1) or with a $Ti_{5c}$-$O_{2c}$ pair (Scheme 2) in a *HCOO* template on $TiO_2$(a)(1 0 1). The energies are referenced to HCOOH(g) and the *HCOO*-saturated surface. The corresponding structures are shown in Figs. 8 and 9 for the routes involve $H^+$-$O_{2c}$ and $Ti_{5c}$-$O_{2c}$ pairs, respectively.

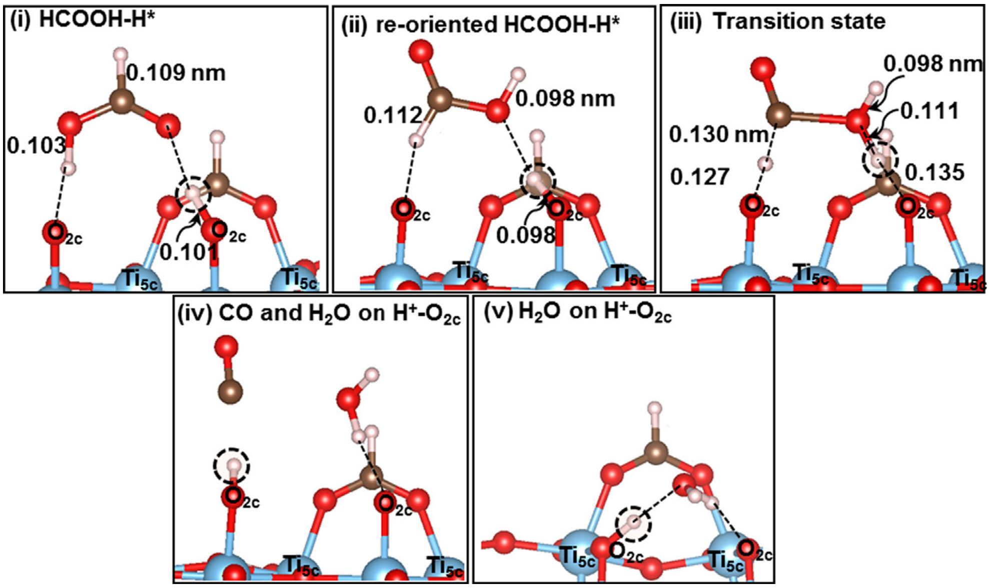

**Fig. 8.** DFT-derived structures of intermediates and TS involved in HCOOH dehydration via reactions with a $H^+$-$O_{2c}$ pair (Scheme 1) in a *HCOO* template on $TiO_2$(a)(1 0 1). The bond distances are shown in the unit of nm.

reconstructing the full bidentate template and completing a catalytic turnover. $H_2O$ molecule formed can reabsorb at the proton (step 6; Scheme 2), competing with HCOOH adsorption (step 1; Scheme 2), which leads to dehydration turnover rates that decrease with increasing $H_2O$ pressure (Fig. 2b).

Both routes in Schemes 1 and 2 involve the formation of HCOOH-H* via molecular HCOOH adsorption at a proton in the *HCOO* template (step 1; Schemes 1 and 2); the equilibrium constant for this step ($K_1$) is reflected in the β parameter in Eq. (1). The magnitude and temperature dependences of $K_1$ are given by the free energy change for such a step ($\Delta G_1$):

$$K_1 = \exp\left(\frac{-\left(G_{HCOOH-H*} - G_{H*} - G_{HCOOH(g)}\right)}{RT}\right) = \exp\left(\frac{-\Delta G_1}{RT}\right), \qquad (3)$$

where $G_{HCOOH\text{-}H*}$, $G_{H*}$, and $G_{HCOOH(g)}$ represent the free energies of HCOOH-H*, the *HCOO*-saturated template, and HCOOH(g), respectively. DFT-derived free energy change for HCOOH-H* formation from HCOOH(g) ($\Delta G_1$; step 1 in Schemes 1 and 2) quantitatively agrees with the value derived from the regressed β parameter (−23 vs. −22 ± 4 kJ mol$^{-1}$; 433 K; Table 3), suggesting that HCOOH-H* species present as MASI during dehydration catalysis and that such species reach saturation coverage at high HCOOH pressures, causing dehydration turnover rates to reach constant values (Fig. 2a). Such mechanistic interpretation also agrees well with infrared measurements that confirmed the identity and surface coverages of HCOOH-H* species that vary in a manner consistent with the effects of HCOOH pressure on dehydration turnover rates (Section 3.2).

The two routes described in Schemes 1 and 2 lead to the same functional form of the rate equation (Eq. (1); derivation in SI; Section S2) that accurately describes all rate data (Fig. 2) and share a common HCOOH-H* precursor. Consequently, these two pathways cannot be distinguished from kinetic or spectroscopic inquiries and differ only in the chemical origin of the α parameter in Eq. (1) and, therefore, in the magnitude of the activation barrier that determines its value. This α parameter divided by the β value (α/β) in Eq. (1) reflects the zero-order rate constant ($k_d$) that is set by the free energy of the kinetically-relevant TS ($G_3^{\ddagger}$; step 3 in Schemes 1 and 2) referenced to the HCOOH-H* precursor:

$$k_d = \frac{k_B T}{h} \exp\left(\frac{-\left(G_3^{\ddagger} - G_{HCOOH-H*}\right)}{RT}\right), \qquad (4)$$

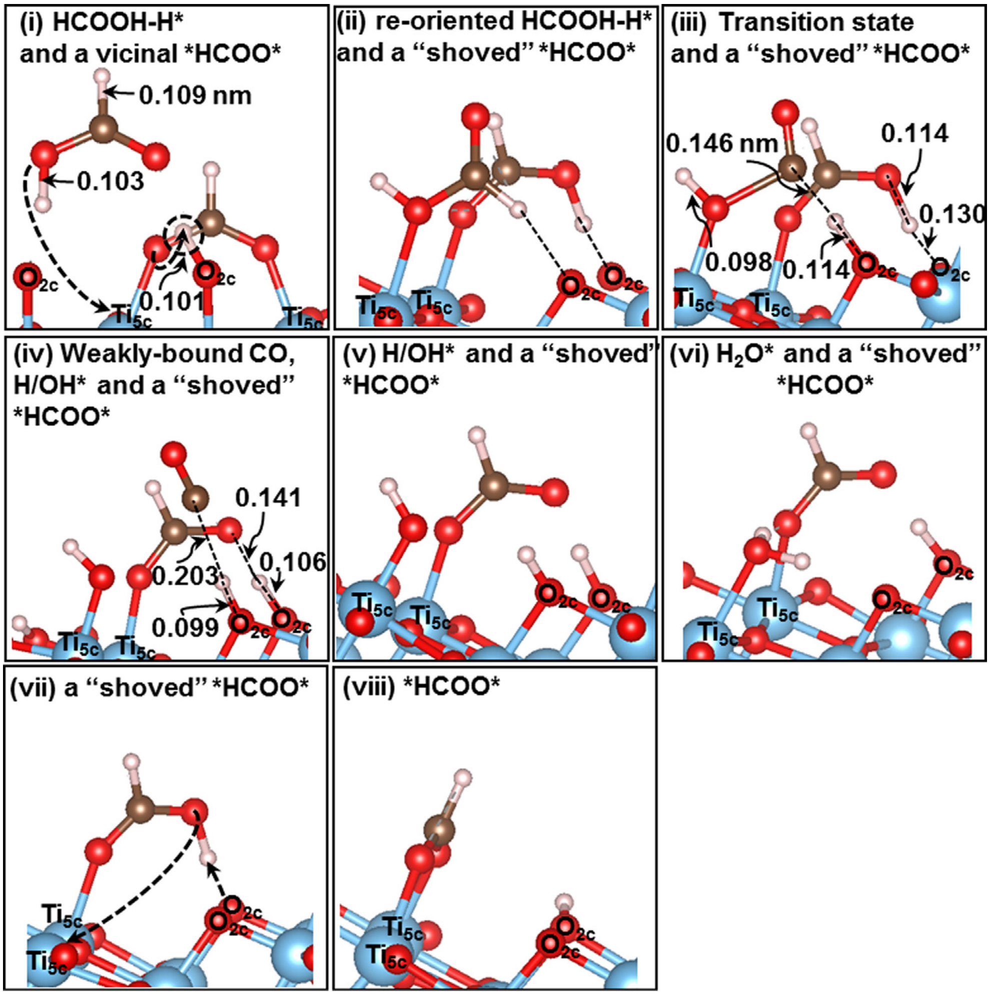
(i) HCOOH-H* and a vicinal *HCOO*
(ii) re-oriented HCOOH-H* and a "shoved" *HCOO*
(iii) Transition state and a "shoved" *HCOO*
(iv) Weakly-bound CO, H/OH* and a "shoved" *HCOO*
(v) H/OH* and a "shoved" *HCOO*
(vi) $H_2O$* and a "shoved" *HCOO*
(vii) a "shoved" *HCOO*
(viii) *HCOO*

**Fig. 9.** DFT-derived structures of intermediates and TS involved in HCOOH dehydration via reactions with a $Ti_{5c}$-$O_{2c}$ pair (Scheme 2) in a *HCOO* template on $TiO_2$(a)(1 0 1). The bond distances are shown in the unit of nm.

**Table 3**
HCOOH dehydration rate parameters ($K_1$ and $k_d$) and the corresponding free energies, enthalpies and entropies (via Eqs. (3) and (4)) estimated from kinetic experiments and from DFT methods for $TiO_2$(a).

| | Exp[a] | Theory[b] | |
|---|---|---|---|
| $K_{1,\ 433K}$ ($kPa^{-1}$) | 4.8 ± 0.4 | | |
| $\Delta G_{,\ 433K}$ ($kJ\ mol^{-1}$) | −22 ± 4 | −23 | |
| $\Delta H_{ads,HCOOH}$ ($kJ\ mol^{-1}$) | −90 ± 20 | −85 | |
| $\Delta S_{ads,HCOOH}$ ($J\ K^{-1} mol^{-1}$) | −160 ± 50 | −143 | |
| | | at $H^+$-$O_{2c}$ pairs | at $Ti_{5c}$-$O_{2c}$ pairs |
| $k_{d,\ 433K,}$($s^{-1}$) | 0.023 ± 0.002 | | |
| $\Delta G^{\ddagger}_{433K}$ ($kJ\ mol^{-1}$) | +121 ± 2 | +151 | +109 |
| $\Delta H^{\ddagger}$ ($kJ\ mol^{-1}$) | +105 ± 8 | +143 | +106 |
| $\Delta S^{\ddagger}$ ($J\ K^{-1}\ mol^{-1}$) | −40 ± 20 | −18 | −7 |

[a] Uncertainties reflect 95% confidential intervals.
[b] Free energies are calculated at 433 K and standard pressure (1 bar).

**Table 4**
Kinetic isotopic effects for the zero-order rate constant ($k_d$) measured on $TiO_2$(a) (at 433 K). DFT-derived values for the routes involving $H^+$-$O_{2c}$ and $Ti_{5c}$-$O_{2c}$ pairs (Schemes 1 and 2) are also listed.

| | Exp.[a] | Theory[b] | |
|---|---|---|---|
| | | at $H^+$-$O_{2c}$ pairs | at $Ti_{5c}$-$O_{2c}$ pairs |
| HCOOH/HCOOD | 1.6 ± 0.2 | 1.2 | 1.4 |
| HCOOH/DCOOH | 3.0 ± 0.4 | 2.3 | 2.0 |
| HCOOH/DCOOD | 3.3 ± 0.4 | 2.8 | 2.8 |

[a] Uncertainties reflect 95% confidential intervals. The $k_d$ values were estimated by regressing the rate data in Fig. 3 to the functional form of Eq. (1).
[b] Free energies are calculated at 433 K and standard pressure (1 bar).

where $k_B$ is Boltzmann's constant, $h$ is Planck's constant, and $R$ is the gas constant.

KIE for this rate constant ($k_d$) reflects the change in the free energy of the kinetically-relevant TS ($G^{\ddagger}_3$; Figs. 8iii and 9iii) respect to its HCOOH-H* precursor ($G_{HCOOH\text{-}H^*}$) when H-atoms in HCOOH are labeled with D-atoms; DFT-derived KIE values are compared to experimental values in Table 4. The kinetically-relevant transition states involved in both routes include the C–H bonds that are partially cleaved (0.130 and 0.146 nm for the routes involve $H^+$-$O_{2c}$ and $Ti_{5c}$-$O_{2c}$ pairs, respectively; Figs. 8iii and 9iii) from the reactant state of HCOOH-H* (0.109 nm; Figs. 8i and 9i). The replacement of this C–H bond in HCOOH with a C–D bond decreases the zero-point vibration energy of its stretching mode in the reactant state (HCOOH-H*) but not at the TS as this mode lies along the reaction coordinate. As a result, DFT-derived KIE values for the $k_d$ constant are much larger than unity for (HCOOH/DCOOH) (2.3 and 2.0 for the routes involve $H^+$-$O_{2c}$ and $Ti_{5c}$-$O_{2c}$ pairs, respectively; 433 K; Table 4), as expected from the experimental observation (3.0 ± 0.4; 433 K; Table 4). In contrast, the O–H bond in HCOOH-H* remains nearly unperturbed at the kinetically-relevant transition states for both routes (0.101 nm vs. 0.098 nm; Figs. 8i and 9i vs. Figs. 8iii and 9iii); the substitution of the H-atom in the O–H bond with the D-atom thus decreases the zero-point energy of its stretching mode in HCOOH-H* and in the transition states to a similar extent. Consequently, KIE is much weaker for HCOOD; DFT-derived $k_d$ constant ratios for HCOOH/HCOOD are closer to unity for both routes (1.2 and 1.4 for the routes involve $H^+$-$O_{2c}$ and $Ti_{5c}$-$O_{2c}$ pairs, respectively; 433 K; Table 4), similar to the experimental KIE (1.6 ± 0.2; 433 K; Table 4). Both routes give KIE values that agree well with experimental observations; these two pathways, thus, also cannot be discerned from isotopic measurements. DFT-derived free energy of the kinetically-relevant TS respect to the HCOOH-H* precursor, however, is much smaller for the route that involves a $Ti_{5c}$-$O_{2c}$ pair (Scheme 2) than a $H^+$-$O_{2c}$ pair (Scheme 1) ($\Delta G^{\ddagger}$ = 109 vs. 151 kJ $mol^{-1}$; 433 K; Table 4) and is also closer to the experimental value (+121 ± 2 kJ $mol^{-1}$; 433 K; Table 4), suggesting the preferential involvement of the route involving a $Ti_{5c}$-$O_{2c}$ pair (Scheme 2).

The enthalpic components of free energies are obtained from the regressed rate parameters measured at a range of temperatures (423–463 K; Fig. 2), which are then used to calculate the corresponding free energies, enthalpies, and entropies (via Eqs. (3) and (4) and G = H - TS) (Table 3). These enthalpy values can be directly compared to DFT-derived electronic energies after corrections of zero-point energies and thermal contributions at the reaction temperatures, without the entropy estimates required for free energy comparisons; these DFT-derived entropy estimates are seldom accurate because they depend sensitively on low-frequency vibrational modes that cannot be properly described by harmonic oscillator models. The measured enthalpy change for HCOOH-H* formation from HCOOH(g) (step 1; Schemes 1 and 2) is very similar to the value derived from DFT ($\Delta H$ = −90 ± 20 vs. −85 kJ $mol^{-1}$; Table 3). The measured enthalpic barrier also agrees well with the value obtained from DFT method for the route involving a $Ti_{5c}$-$O_{2c}$ pair (Scheme 2) ($\Delta H^{\ddagger}$ = +105 ± 8 vs. +106 kJ $mol^{-1}$; Table 3) but is significantly smaller than the value calculated for the route involving a $H^+$-$O_{2c}$ pair (Scheme 1) (+143 kJ $mol^{-1}$; Table 3), thus supporting the predominant involvement of $Ti_{5c}$-$O_{2c}$ sites that act as Lewis acid-base pairs for HCOOH dehydration turnovers on the *HCOO*-saturated $TiO_2$(a) template.

DFT-derived energies, taken together with their comparisons to experimental values, lead us to conclude that HCOOH dehydration turnovers on the $TiO_2$(a) surfaces occur via HCOOH-H* intermediates that are formed upon molecular HCOOH adsorption at protons in the *HCOO* template. These HCOOH-H* species eliminate $H_2O$ by reacting with $Ti_{5c}$-$O_{2c}$ pairs, made available by temporarily detaching the O-atoms from the $Ti_{5c}$ centers in *HCOO* template. The possible involvement of such dehydration routes on $TiO_2$(r) is discussed next.

### 3.5. Mechanistic details of HCOOH dehydration on rutile $TiO_2$

HCOOH dehydration rates measured on the $TiO_2$(r) sample also follow the Langmuirian behavior (433–463 K; 0.1–3 kPa HCOOH; Fig. S8; SI), as in the case of $TiO_2$(a) (Fig. 2); these rate data were used to regress the rate parameters ($\alpha$, $\beta$, $\gamma$; Eq. (1)). The measured zero-order rate constants ($k_d = \alpha/\beta$) for $TiO_2$(a) and $TiO_2$(r) catalysts are shown in Fig. 10 as a function of reciprocal temperatures (423–463 K); this $k_d$ parameter would reflect the free energy of the kinetically-relevant TS relative to the HCOOH-H* precursor (via Eq. (4)) if HCOOH dehydration turnovers on $TiO_2$(a) and $TiO_2$(r) involve the same elementary steps (Schemes 1 and 2). The $k_d$ values measured on $TiO_2$(r) are an order of magnitude smaller than those for $TiO_2$(a); yet, the slopes, which reflect the enthalpy of the kinetically-relevant TS relative the HCOOH-H* precursor, were similar between the two catalysts ($\Delta H^{\ddagger}$ = 99 ± 3 vs. 105 ± 8 kJ $mol^{-1}$ for $TiO_2$(r) and $TiO_2$(a), respectively). The similar enthalpic barriers on two $TiO_2$ samples with dramatically different turnover rates seem to suggest that the residual anatase phase that presents as small aggregates in the $TiO_2$(r) sample is responsible for the measured dehydration reactivity; these anatase-like structures in the $TiO_2$(r) sample are undetectable from XRD patterns (Fig. S2; SI) but have been previously implicated for low but measurable reactivity of the $TiO_2$(r) sample in aldol condensation [45] and ketonization of acids [26]. The identities and surface coverages of HCOOH-derived species on $TiO_2$(r) surfaces are assessed next from infrared inquiries during dehydration catalysis and during the decomposition of pre-adsorbed HCOOH-derived species upon temperature ramping.

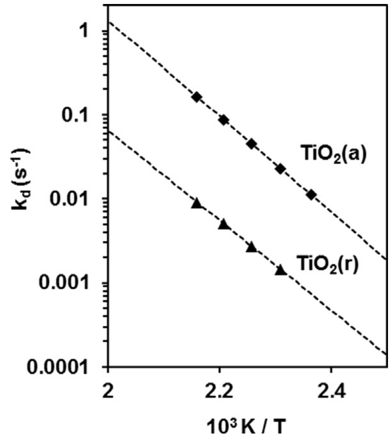

**Fig. 10.** Measured zero-order dehydration rate constants as a function of reciprocal temperature (423–463 K) for $TiO_2$(a) and $TiO_2$(r) catalysts.

#### 3.5.1. The identity and surface coverages of bound species formed upon contact of $TiO_2$(r) with HCOOH

Fig. 11a shows the infrared spectra collected during HCOOH dehydration on $TiO_2$(r) (433 K; 1.5 kPa HCOOH). Besides the bands for HCOOH(g) (1792, 1757, 1218, 1120, and 1088 $cm^{-1}$; Table 1), distinct bands at 1541 and 1370 $cm^{-1}$ appeared, which are assigned to antisymmetric and symmetric COO stretching modes of *HCOO* from DFT-derived frequencies (1519 and 1339 $cm^{-1}$; Table 1). The intensities of these bands for *HCOO* species (at 1541 and 1370 $cm^{-1}$) remain unchanged upon the removal of HCOOH(g) from the inlet stream; they persisted even after 7.1 ks, the time scale that is much larger the time required to decompose 90% of bound intermediate (2.3 ks), estimated by assuming first-order decomposition and from measured zero-order rate at 433 K (calculation details in Section S2; SI). This observation indicates the inactive nature of *HCOO* on $TiO_2$(r) during HCOOH dehydration turnovers (at 433 K), as in the case of $TiO_2$(a) (Section 3.2). The integrated intensities of the distinct *HCOO* band at 1541 $cm^{-1}$ (normalized by the value at 1.8 kPa HCOOH) remain unaffected as HCOOH pressures increase from 0.1 to 1.8 kPa (433 K; Fig. 11b). Such results contradict the Langmuirian behavior of observed rates (433 K; 0.1–3 kPa HCOOH; Fig. S8; SI), which, in turn, suggest the involvement of other bound species that vary in coverage over the range of HCOOH pressures that does not affect the coverage of *HCOO*.

The small bands at 1678 $cm^{-1}$ and 1210 $cm^{-1}$ are also detectable on $TiO_2$(r), which are assigned to C=O and C–O stretching modes of a molecular HCOOH bound at a proton (HCOOH-H*) in *HCOO* template, consistent with DFT-derived frequencies (1665 $cm^{-1}$ and 1218 $cm^{-1}$; Table 1). The intensities of these HCOOH-H* bands decrease upon the removal of HCOOH(g) from the reactant stream, but much slowly than those expected from measured dehydration turnover rates; these bands remain even after 7.1 ks in the flowing He stream, persisting much longer than

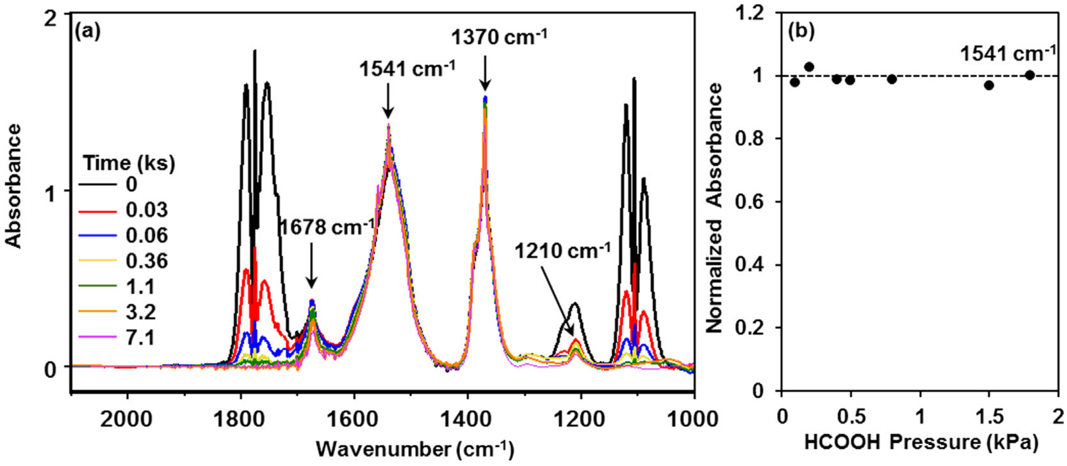

**Fig. 11.** (a) Infrared spectra of $TiO_2$(r) during steady-state HCOOH dehydration (1.5 kPa HCOOH; 433 K) and after the removal of HCOOH(g) from the reactant stream (0.03–7.1 ks). The spectrum of the $TiO_2$(r) sample measured at 433 K in flowing He after its treatment in $O_2$ (20 kPa; 573 K; 0.5 h) was taken as a reference. (b) The integrated absorbance for the 1541 $cm^{-1}$ band (for *HCOO*) (●) as a function of HCOOH pressure (0.1–1.8 kPa; 433 K), normalized by the maximum value at the highest HCOOH pressure (1.8 kPa) used in these experiments.

the estimated time required to decompose 90% of bound intermediates (2.3 ks; calculation details in Section S2; SI). These results may indicate that weakly-bound HCOOH-H* species formed on minor surfaces (undetectable for infrared) are responsible for measured dehydration turnovers. The small intensities of these bands at 1678 $cm^{-1}$ and 1210 $cm^{-1}$ also impose difficulties in assessing the effect of HCOOH pressure on their integrated intensities, which reflect the surface coverage of these HCOOH-H* species (the spectra collected at 0.1–1.8 kPa HCOOH pressures in Fig. S9; SI). The surface densities of *HCOO* and HCOOH-H* species formed on $TiO_2$(r) surfaces are assessed next by counting the number of HCOOH and CO molecules evolved upon heating those species pre-adsorbed on $TiO_2$(r) powders (TPD/TPSR).

HCOOH, CO and $H_2O$ molecules desorb as $TiO_2$(r) exposed to HCOOH (0.5 kPa; ambient temperature) is heated (from ambient temperature to 700 K) in flowing He. The amounts desorbed correspond to 0.83 HCOOH per surface $Ti_{5c}$-$O_{2c}$ site pair. Infrared spectra of $TiO_2$(r) collected upon the contact with 0.5 kPa HCOOH at 300 K detect *HCOO* and HCOOH-H* species (Fig. S5b; SI). The *HCOO* band (1541 $cm^{-1}$) weakens only above 500 K (Fig. 12a), leading to the formation of CO (and $H_2O$) (Fig. 12c). The band for HCOOH-H* at 1678 $cm^{-1}$, in contrast, diminishes monotonically from 300 K and disappears above 500 K (Fig. 12b), as these species desorb as unreacted HCOOH or as CO (and $H_2O$) products (Fig. 12c). The CO evolution feature above 500 K thus corresponds to *HCOO* decomposition as HCOOH-H* species are absent at these temperatures (>500 K; Fig. 12b). The deconvolution of CO peaks and the integration of the CO feature above 500 K give the *HCOO*/$Ti_{5c}$-$O_{2c}$ ratio of 0.55, which agrees well with the stoichiometry expected for saturation of all $Ti_{5c}$ centers with *HCOO*.

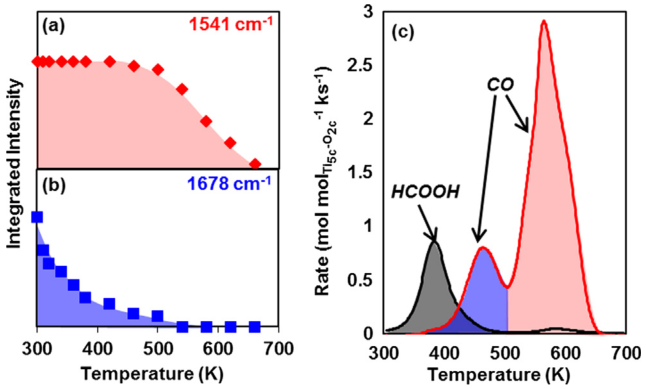

**Fig. 12.** The integrated absorbance for the infrared bands at (a) 1541 $cm^{-1}$ (for *HCOO*) and (b) 1678 $cm^{-1}$ (for HCOOH-H*) and (c) the HCOOH and CO evolution rates as a function of temperature (300–700 K) measured upon heating (in flowing He) the $TiO_2$(r) sample containing pre-adsorbed HCOOH-derived species.

The saturation of all $Ti_{5c}$ centers in $TiO_2$(r) with *HCOO* limits the binding of molecular HCOOH on such $Ti_{5c}$ centers; each *HCOO* formation, however, adds one proton at the surface $O_{2c}$-atom, on to which molecular HCOOH can bind to form HCOOH-H* that is responsible for the 1678 $cm^{-1}$ band. These HCOOH-H* species present at a HCOOH/ $Ti_{5c}$-$O_{2c}$ stoichiometry of 0.28 that is much smaller than the value expected from the number of protons that present as pair of *HCOO* (0.55). These results suggest that HCOOH-H* species are formed at the protons in the minor surfaces in the $TiO_2$(r) sample. Such mechanistic interpretation agrees with DFT-derived adsorption free energy of HCOOH-H* species at protons in *HCOO*-saturated $TiO_2$(r)(1 1 0), which is less negative than that for $TiO_2$(a)(1 0 1) ($\Delta G_{ads} = -13$ vs. $-23$ kJ $mol^{-1}$; 1/4 ML; 433 K); these DFT results are discussed in detail next.

### *3.5.2. Theoretical assessments of elementary steps involved in HCOOH dehydration on *HCOO*-saturated $TiO_2$(r)*

DFT-derived free energy change of forming *HCOO* from HCOOH(g) on the $TiO_2$(r)(1 1 0) surface is large and negative ($\Delta G_{ads} = -71$ kJ $mol^{-1}$; 1/8 ML; 433 K; Fig. 13a; Table 5), consistent with the presence of inactive *HCOO* template on $TiO_2$(r) during dehydration catalysis. This free energy change becomes less negative from $-71$ to $-63$ kJ $mol^{-1}$ as *HCOO* coverage increases from 1/8 ML (no neighboring *HCOO*) to its saturation 1/2 ML coverage (433 K; Table 5). This trend contradicts negligible adsorbate-adsorbate repulsions within *HCOO* template on the $TiO_2$(a)(1 0 1) surface, evident from small variance in the *HCOO* formation free energy that varies only from $-57$ to $-54$ kJ $mol^{-1}$ for 1/8 ML to 1/2 ML coverages (Table 2). The stronger *HCOO* coverage effect for the $TiO_2$(r)(1 1 0) surface reflects the denser spacing between bound *HCOO* species in $TiO_2$(r)(1 1 0) than in $TiO_2$(a)(1 0 1); the shortest distance between neighboring *HCOO* in *HCOO*-saturated $TiO_2$(r)(1 1 0) is 0.37 nm, compared to 0.52 nm for $TiO_2$(a)(1 0 1), due to its shorter $Ti_{5c}$-$Ti_{5c}$ distances (0.296 vs. 0.379 nm for $TiO_2$(r)(1 1 0) and $TiO_2$(a)(1 0 1), respectively). The *HCOO* formation free energy for $TiO_2$(r)(1 1 0),

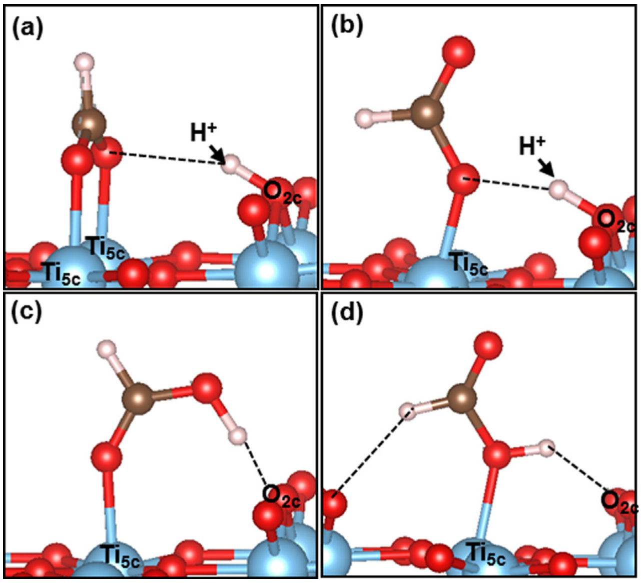

**Fig. 13.** DFT-derived HCOOH binding modes on $TiO_2$(r)(1 1 0): (a) bidentate formate, (b) monodentate formate, and (c) molecularly bound HCOOH at a $Ti_{5c}$ center (HCOOH*) via its C=O group and (d) via its O–H group.

however, is more negative than for $TiO_2$(a)(1 0 1) even at 1/2 ML coverage ($\Delta G_{ads}$ = −63 vs. −54 kJ $mol^{-1}$; 1/2 ML; 433 K) because of i) the stronger acid strength of $Ti_{5c}$ centers in $TiO_2$(r)(1 1 0), evident from their more negative DFT-derived $OH^-$ binding energies (−369 vs. −246 kJ $mol^{-1}$ for $Ti_{5c}$ centers in $TiO_2$(r)(1 1 0) and $TiO_2$(a)(1 0 1), respectively [26]), and ii) the additional stabilization of *HCOO* on $TiO_2$(r)(1 1 0) via H-bonding with the proton on the vicinal $O_{2c}$ (Fig. 13a); this proton in $TiO_2$(a)(1 0 1) prefers to interact with another $O_{2c}$ center than with *HCOO* (Fig. 6a).

DFT-derived free energy changes for the formation of monodentate formate and molecular HCOOH bound at a $Ti_{5c}$ center (via its C=O or O–H groups) from HCOOH(g) are much less negative than that of bidentate formate ($\Delta G_{ads}$ = −4, −49, −12 vs. −71 kJ $mol^{-1}$; 1/8 ML; 433 K; Fig. 13; Table 5). These results are consistent with the preferential formation of *HCOO* species upon HCOOH adsorption on $TiO_2$(r) that leads to the formation of stable *HCOO* template during HCOOH dehydration turnovers. This *HCOO* template is inactive but provides stoichiometric 1/2 ML protons that may act as binding points for molecular HCOOH adsorption to form HCOOH-H* species (Sections 3.2–3.4). DFT-derived HCOOH-H* formation free energy is less negative for $TiO_2$(r)(1 1 0) than for $TiO_2$(a)(1 0 1) ($\Delta G_{ads}$ = −13 vs. −23 kJ $mol^{-1}$; 1/4 ML; 433 K) due to the energetic penalty associated with the interruption of H-bonding between *HCOO* and the proton upon HCOOH-H* formation; such H-bonding is absent in the *HCOO*-template on $TiO_2$(a)(1 0 1) (Fig. 6a). These results are consistent with the measured surface density of HCOOH-H* species on the $TiO_2$(r) sample (0.28 HCOOH per $Ti_{5c}$-$O_{2c}$ site pair) that is much lower than the number of protons present as pairs of *HCOO* (0.55 $H^+$ per $Ti_{5c}$-$O_{2c}$ site pair) (Section 3.5.1.).

The *HCOO* template on the $TiO_2$(r)(1 1 0) surface is also less active for HCOOH dehydration turnovers than that on $TiO_2$(a)(1 0 1), as shown by measured zero-order rate constants that are an order of magnitude smaller for $TiO_2$(r) than for $TiO_2$(a) (Fig. 10). The origin of its low reactivity is discussed next from DFT-derived free energies of intermediates and transition states involved in the dehydration turnovers (Fig. 14); these energies are calculated at 433 K and standard HCOOH pressure (1 bar) and referenced to the reactant state of HCOOH(g) and *HCOO*-saturated $TiO_2$(r)(1 1 0). Free energies are reported at 1/4 ML HCOOH-H* coverage but are expected to be similar at higher coverages as interactions among adsorbates are small, inferred by the free energy change for HCOOH-H* formation from HCOOH(g) that varies by < 2 kJ $mol^{-1}$ between 1/8 ML (isolated HCOOH-H*) and 1/2 ML (saturation) coverages (Fig. S7; SI).

**Table 5**
DFT-derived free energy change for the formation of bidentate and monodentate formates and molecularly bound HCOOH at a $Ti_{5c}$ center (HCOOH*) via its C=O or O–H groups from HCOOH(g) on the $TiO_2$(r)(1 1 0) surface[a].

| Adsorption mode | | Figure | Coverage (ML) | $\Delta G_{ads}$ (kJ $mol^{-1}$) |
|---|---|---|---|---|
| Bidentate formate | | 13a | 1/8 | −71 |
| | | | 1/2 | −63 |
| Monodentate formate | | 13b | 1/8 | −4 |
| molecular HCOOH* | on $Ti_{5c}$ through C=O | 13c | 1/8 | −49 |
| | on $Ti_{5c}$ through O–H | 13d | 1/8 | −12 |

[a] Free energies are derived at 433 K and standard HCOOH pressure (1 bar).

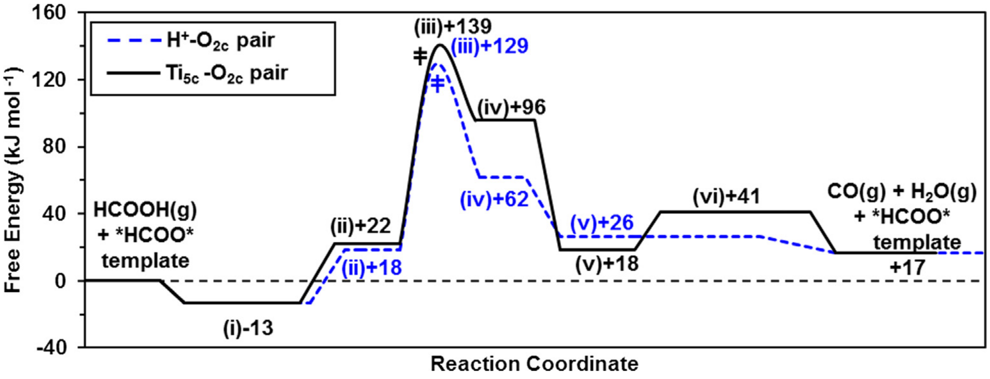

**Fig. 14.** DFT-derived free energies (kJ $mol^{-1}$; 433 K; 1 bar HCOOH) of intermediates and TS involved in HCOOH dehydration via reactions with a $H^+$-$O_{2c}$ pair (Scheme 1) or with a $Ti_{5c}$-$O_{2c}$ pair (Scheme 2) in a *HCOO* template on $TiO_2$(r)(1 1 0). The energies are referenced to HCOOH(g) and the *HCOO*-saturated surface. The corresponding geometries are shown in Figs. S10 and S11 (in SI) for the routes involve $H^+$-$O_{2c}$ and $Ti_{5c}$-$O_{2c}$ pairs, respectively.

The HCOOH-H* species bound at protons in *HCOO*-saturated $TiO_2$(r)(1 1 0) (Figs. S10i and S11i) can eliminate $H_2O$ via reactions with $H^+$-$O_{2c}$ or $Ti_{5c}$-$O_{2c}$ pairs (Schemes 1 and 2); DFT-derived structures of intermediates and transition states involved in these routes are shown in Figs. S10 and S11 (in SI), respectively. The latter route is preferred on the *HCOO*-saturated $TiO_2$(a)(1 0 1) surface, which, in turn, requires the momentary detachment of the O-atom in *HCOO* from a $Ti_{5c}$ center via its reprotonation to form a molecular HCOOH that is bound at a $Ti_{5c}$ center via its C=O group (HCOOH*) (step 2; Scheme 2). The coadsorbed HCOOH-H* then can reorient itself to place its O-atom in the O–H group at the $Ti_{5c}$ center (made available by cleaving one of the two $Ti_{5c}$-O bonds in *HCOO*) and its H-atom in the C-H group on the neighboring $O_{2c}$ center (Fig. S11ii; SI), the configuration that is required to use a $Ti_{5c}$-$O_{2c}$ site pair as a Lewis acid-base pair. This "shoving" step, however, is particularly less favorable for $TiO_2$(r)(1 1 0) than for $TiO_2$(a)(1 0 1) ($\Delta G$ = +35 vs. +8 kJ $mol^{-1}$; 433 K; Figs. 14 and 7, respectively) because of more strongly bound *HCOO* on $TiO_2$(r)(1 1 0) than on $TiO_2$(a)(1 0 1) ($\Delta G_{ads}$ = −63 vs. −54 kJ $mol^{-1}$; 1/2 ML; 433 K). The coadsorbed HCOOH* species, formed via reprotonation of *HCOO* and reorientation of HCOOH-H*, are also less stable on $TiO_2$(r)(1 1 0) because the shorter $Ti_{5c}$-$Ti_{5c}$ distances in $TiO_2$(r)(1 1 0) than in $TiO_2$(a)(1 0 1) (0.296 vs. 0.379 nm) induce greater repulsions between co-adsorbed HCOOH* species. The HCOOH* intermediate formed upon the reorientation of HCOOH-H* cleaves its C–O bond as CO molecule incipiently leaves and the O-atom in the O–H group attacks the acidic $Ti_{5c}$ center; concurrently, the C–H bond in HCOOH* is cleaved upon H-abstraction by the basic $O_{2c}$ center (Fig. S11iv; SI) (step 3; Scheme 2). The TS involved in this step (Fig. S11iii; SI) imposes the highest free energy barrier along the reaction coordinate (Fig. 14), which contains partially cleaved C–O and C–H bonds. The weakly-bound CO formed desorbs and the remaining O–H on the $Ti_{5c}$ center and H at the $O_{2c}$ center recombine to form a molecular $H_2O$ bound at the $Ti_{5c}$ center (Fig. S11v; SI); this step is exoergic with the free energy change of −78 kJ $mol^{-1}$ (433 K; Fig. 14). $H_2O$ formed desorbs in the next endoergic step ($\Delta G_{des}$ = +23; 433 K; Fig. 7) (step 4; Scheme 2) at which the "shoved" HCOOH* deprotonates to reform *HCOO*(Fig. S11vi; SI) ($\Delta G$ = −14 kJ $mol^{-1}$; 433 K; Fig. 7) (step 5; Scheme 2). DFT-derived free energy of the kinetically-relevant TS relative to the HCOOH-H* precursor, which determines the $k_d$ constant in Fig. 10, is very large ($\Delta G^{\ddagger}$ = 152 kJ $mol^{-1}$; 433 K; Fig. 14), compared to the value calculated for $TiO_2$(a)(1 0 1) ($\Delta G^{\ddagger}$ = 109 kJ $mol^{-1}$; 433 K; Fig. 7), consistent with the low dehydration reactivity of the *HCOO* template formed on the $TiO_2$(r) surface (Fig. 10).

HCOOH-H* formed on the *HCOO*-saturated $TiO_2$(r)(1 1 0) surface may instead react with the $H^+$-$O_{2c}$ pair via elementary steps described in Scheme 1. In this route, HCOOH-H* rearranges itself to place its O-atom in the O–H group on the proton and its H-atom in the C–H group on a vicinal $O_{2c}$ center (step 2; Scheme 1; Fig. S10ii). This step is endoergic ($\Delta G$ = +31 kJ $mol^{-1}$; 433 K; Fig. 14) but is required to use the $H^+$-$O_{2c}$ moiety as a Lewis acid-base pair. This rearranged HCOOH-H* cleaves its C–O bond as a CO molecule leaves upon the formation of a $H_2O$ molecule via the transfer of the bound proton to the O–H group in HCOOH-H*. Concurrently, its C–H bond cleaves as the surface $O_{2c}$-atom abstracts the H-atom from HCOOH-H* (step 3; Scheme 1; Fig. S10iv). The TS involved in this step (Fig. S10iii) involves partially cleaved C–O and C–H bonds and imposes the highest free energy barrier along the reaction coordinate (Fig. 14). The weakly-bound CO formed desorb in a subsequent exoergic step ($\Delta G$ = −36 kJ $mol^{-1}$; 433 K; Fig. 14; Fig. S10iv) and a more strongly bound $H_2O$ desorbs in the next step to complete the turnover ($\Delta G$ = −9 kJ $mol^{-1}$; 433 K; Fig. 14; Fig. S10v) (step 4; Scheme 1). DFT-derived free energy of the kinetically-relevant TS for this route relative to the HCOOH-H* precursor is smaller than the route involving the $Ti_{5c}$-$O_{2c}$ pair ($\Delta G^{\ddagger}$ = 142 vs. 152 kJ $mol^{-1}$; 433 K; Fig. 14); yet, this free energy barrier is still much larger than the value calculated for the $TiO_2$(a)(1 0 1) surface ($\Delta G^{\ddagger}$ = 109 kJ $mol^{-1}$ for the route involving the $Ti_{5c}$-$O_{2c}$ pair; 433 K; Fig. 7).

The large magnitude of DFT-derived free energy barrier of forming the kinetically-relevant TS from HCOOH-H* precursor on *HCOO*-saturated $TiO_2$(r)(1 1 0) ($\Delta G^{\ddagger}$ = 142 kJ $mol^{-1}$; 433 K; Fig. 14) predicts undetectable rates at 433 K with estimated $k_d$ constant ($6 \times 10^{-5}$ $s^{-1}$; via Eq. (4)) that is much smaller than the measured $k_d$ constant ($1 \times 10^{-3}$ $s^{-1}$; 433 K; Fig. 10). These results again support that measured rates on the $TiO_2$(r) sample reflect the reactivities of minor impurities present in the rutile sample. The low reactivity of $TiO_2$(r) originates from the stronger acid strength of its $Ti_{5c}$ centers that bind *HCOO* too strongly and its shorter $Ti_{5c}$-$Ti_{5c}$ distances that induce repulsions between co-adsorbed HCOOH* species, which, in turn, impose large energetic penalties to "shove" *HCOO* in the *HCOO* template, the step that is required to use $Ti_{5c}$-$O_{2c}$ sites as a Lewis acid-base pairs.

DFT-derived free energies discussed thus far were calculated by considering stoichiometric $TiO_2$ surfaces. The quantitative agreement between these energies and experimental values implies the lack of involvements of defects for dehydration turnovers. Such conclusion is further supported from the negligible differences in areal rates among $TiO_2$(a) samples containing various contents of such defects, which are discussed in detail in the following section.

### *3.6. The nature of binding and active centers at $TiO_2$(a) surface*

Crystalline $TiO_2$(a) powders were treated in inert (He; 15 h), oxidative (21 kPa $O_2$; 15 h), or reductive streams (20 kPa $H_2$; 1 h) at 723 K before the rate measurements (1.5 kPa HCOOH; 433 K; Fig. 15) in order to vary the number of reduced $Ti^{3+}$ centers, previously proposed as the active structures in HCOOH dehydration [13,24]. $TiO_2$(a) samples treated in He or $O_2$ at 723 K gave similar areal HCOOH dehydration rates (140 μmol $m^{-2}$ $ks^{-1}$; Fig. 15), indicative of the absence of reduced centers in these $TiO_2$ samples or their kinetic irrelevance in dehydration turnovers. Reduced centers were deliberately formed on $TiO_2$(a) by $H_2$ treatment (20 kPa) at 723 K for 1 h [46,47]. Areal rates decreased only slightly by the $H_2$ treatment at 723 K (from 140 to 130 μmol $m^{-2}$ $ks^{-1}$; Fig. 16), because either i) reduced centers do not form during this treatment, ii) such centers are inactive and present at coverages much smaller than for the stoichiometric Ti–O pairs, or iii) reduced centers are re-oxidized by $H_2O$ formed during HCOOH dehydration catalysis. Irrespective of the cause of this insensitivity to reductive treatments, these data show that such treatments do not form

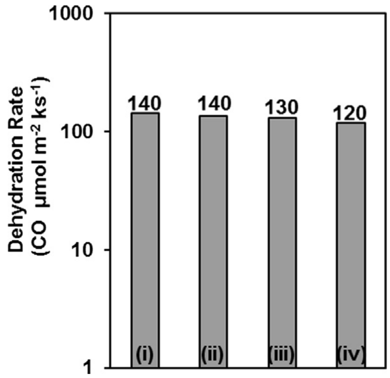

**Fig. 15.** Areal HCOOH dehydration rates (1.5 kPa HCOOH, 433 K) measured on $TiO_2$(a) after their treatments in (i) He (723 K), (ii) 21 kPa $O_2$ (723 K), (iii) 20 kPa $H_2$ (723 K) and (iv) 20 kPa $H_2$ (823 K).

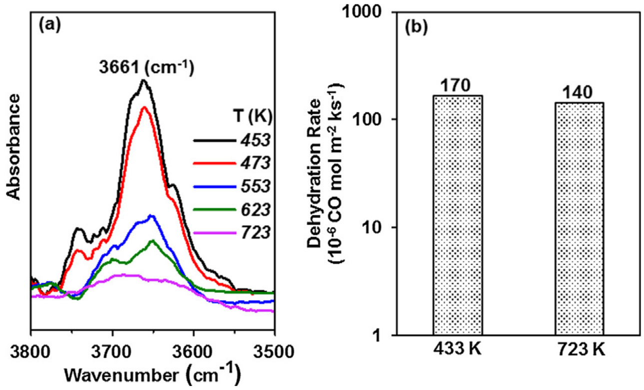

**Fig. 16.** (a) Infrared spectra collected during the thermal treatment of $TiO_2$(a) in flowing He (453–723 K) and (b) areal HCOOH dehydration rates measured on $TiO_2$(a) (433 K; 1.5 kPa HCOOH) after the thermal treatments in flowing He at 433 K (left) and 723 K (right).

active centers that contribute to measured rates. A $H_2$ (20 kPa) treatment at higher temperature (823 K) for 1 h decreased areal rates to a slightly larger extent (from 140 to 120 μmol $m^{-2}$ $ks^{-1}$, compared to the samples treated in $O_2$; Fig. 16); these areal rates were not recovered after $O_2$ exposure at 723 K for 2 h (Fig. S3a; SI). The fractional content of $TiO_2$(r) in the $TiO_2$(a) sample (the ratio between $TiO_2$(r) and $TiO_2$(a) phases) increases from 11 to 14 % upon the reductive treatment at 823 K, evidenced by the phase quantification of X-ray diffractograms measured on the $TiO_2$(a) samples before and after such $H_2$-treatment (Fig. S1; SI). Thus, observed decrease in areal rates seems to reflect the partial conversion of anatase phase in the $TiO_2$(a) sample into rutile, a phase that is much less active than anatase.

The kinetic involvement of titanols that present as defects in $TiO_2$(a) samples for HCOOH dehydration turnovers was ruled out from the catalytic consequences of treatments that vary their surface densities, as detected from infrared spectra. The intensity of the O–H stretching mode of titanols (3661 $cm^{-1}$) decreases as vicinal OH groups recombine to form $H_2O$ with increasing temperature in a He flow and becomes undetectable above 723 K on $TiO_2$(a) (Fig. 16a). Areal rates are similar on $TiO_2$(a) treated at 433 and 723 K (1.5 kPa HCOOH; 433 K; Fig. 16b), which show markable different intensities of O–H stretch from the infrared spectra. These data indicate that titanols, which present as minor defects at $TiO_2$ surfaces treated at mild temperature (423 K), are not involved in dehydration turnovers.

## 4. Conclusions

HCOOH decomposes on $TiO_2$ surfaces to form CO and $H_2O$ products without detectable formation of dehydrogenation products ($CO_2$ and $H_2$) (423–463 K; 0.1–3 kPa HCOOH). Dehydration turnovers are mediated by $Ti_{5c}$-$O_{2c}$ site pairs on stoichiometric $TiO_2$ surfaces. These $Ti_{5c}$ centers, however, are saturated with inactive *HCOO* species at conditions relevant to catalysis (423–463 K; 0.1–3 kPa HCOOH), evidenced by in-situ infrared spectra and the quantitative assessment of *HCOO* on $TiO_2$ surfaces from TPD/TPSR measurements. Such *HCOO* species form a stable and inactive organic template that contains stoichiometric amount of protons, onto which HCOOH binds molecularly (HCOOH-H*) to form a coexisting adlayer. The $H_2O$ elimination from this reactive HCOOH-H* intermediate is the sole-kinetically-relevant step. Such step involves its interaction with a $Ti_{5c}$-$O_{2c}$ site pair, which, in turn, requires a momentary detachment of the O-atom in *HCOO* from the $Ti_{5c}$ center by re-protonating *HCOO* to form molecularly bound HCOOH*. This "shoving" step is much less favorable for $TiO_2$(r) than for $TiO_2$(a) because i) the stronger acid strength of $Ti_{5c}$ centers in $TiO_2$(r) bind *HCOO* too strongly and ii) the shorter $Ti_{5c}$-$Ti_{5c}$ distances in $TiO_2$(r) induce greater repulsions between co-adsorbed HCOOH* species formed upon the re-protonation step. These differences account for a very low and undetectable dehydration reactivity of $TiO_2$(r) at examined conditions (423–463 K; 0.1–3 kPa HCOOH). The proposed pathways involving stoichiometric $Ti_{5c}$-$O_{2c}$ pairs are consistent with all experimental findings and give DFT-derived energies and kinetic isotopic effects that quantitatively agree with experimental values without the need of defects. The lack of involvements of defects in dehydration catalysis is also supported by the negligible differences in areal rates among $TiO_2$(a) samples containing various contents of defects, such as O-vacancies and isolated titanols.

## Declaration of Competing Interest

The authors declare that they have no known competing financial interests or personal relationships that could have appeared to influence the work reported in this paper.

## Acknowledgement

The authors thank Drs. Biswanath Dutta and Xueqiang (Alex) Zhang at the University of California at Berkeley for their help in collecting X-ray diffractograms and Dr. Unai De La Torre for his careful proofreading of the manuscript. This work has been supported by the U.S. Department of Energy (DOE), Office of Science, Office of Basic Energy Sciences (Contract No. DE-AC05-76RL0-1830). This research was achieved using the resources at EMSL facilities (the project number of 48772), a DOE Office of Science User Facility sponsored by the Office of Biological and Environmental Research. This work also used the computational resources at the National Energy Research Scientific Computing Center (NERSC), a U.S. Department of Energy Office of Science User Facility operated under Contract No. DE-AC02-05CH1123 and at the Extreme Science and Engineering Discovery Environment (XSEDE) [48], supported by National Science Foundation (grant number ACI-1548562).

## Appendix A. Supplementary material

Supplementary data to this article can be found online at https://doi.org/10.1016/j.jcat.2019.12.043.

## References

[1] A. Ueno, T. Onishi, K. Tamaru, Dynamic technique to elucidate the reaction intermediate in surface catalysis. Water-gas shift reaction, Trans. Faraday Soc. 66 (1970) 756–763, https://doi.org/10.1039/tf9706600756.

[2] J.L. Robbins, E. Iglesia, C.P. Kelkar, B. DeRites, Methanol synthesis over Cu/SiO2 catalysts, Catal. Letters. 10 (1991) 1–10, https://doi.org/10.1007/BF00764730.

[3] M. Shekhar, J. Wang, W.-S. Lee, W.D. Williams, S.M. Kim, E.A. Stach, et al., Size and Support Effects for the Water-Gas Shift Catalysis over Gold Nanoparticles Supported on Model $Al_2O_3$ and $TiO_2$, J. Am. Chem. Soc. 134 (2012) 4700–4708, https://doi.org/10.1021/ja210083d.

[4] P. Panagiotopoulou, A. Christodoulakis, D.I. Kondarides, S. Boghosian, Particle size effects on the reducibility of titanium dioxide and its relation to the water-gas shift activity of Pt/$TiO_2$ catalysts, J. Catal. 240 (2006) 114–125, https://doi.org/10.1016/j.jcat.2006.03.012.

[5] M. Ojeda, E. Iglesia, Formic Acid Dehydrogenation on Au-Based Catalysts at Near-Ambient Temperatures, Angew. Chemie. 121 (2009) 4894–4897, https://doi.org/10.1002/ange.200805723.

[6] J. Scaranto, M. Mavrikakis, HCOOH decomposition on Pt(111): A DFT study, Surf. Sci. 648 (2016) 201–211, https://doi.org/10.1016/j.susc.2015.09.023.

[7] J.A. Herron, J. Scaranto, P. Ferrin, S. Li, M. Mavrikakis, Trends in Formic Acid Decomposition on Model Transition Metal Surfaces: A Density Functional Theory study, ACS Catal. 4 (2014) 4434–4445, https://doi.org/10.1021/cs500737p.

[8] J.M. Trillo, G. Munuera, J.M. Criado, Catalytic Decomposition of Formic Acid on Metal Oxides, Catal. Rev. 7 (1972) 51–86, https://doi.org/10.1080/01614947208064710.

[9] G. Munuera, A study of the mechanisms of formic acid dehydration on $TiO_2$, J. Catal. 18 (1970) 19–29, https://doi.org/10.1016/0021-9517(70)90306-4.

[10] P. Mars, J.J.F. Scholten, P. Zwietering, The catalytic decomposition of formic acid, Adv. Catal. 14 (1963) 35–113, https://doi.org/10.1016/S0360-0564(08)60338-7.

[11] H. Onishi, T. Aruga, Y. Iwasawa, Switchover of Reaction Paths in the Catalytic Decomposition of Formic Acid on $TiO_2$(110) Surface, J. Catal. 146 (1994) 557–567, https://doi.org/10.1006/jcat.1994.1094.

[12] M.A. Enriquez, J.P. Fraissard, Dehydration of formic acid on titanium dioxides. Nature of active centers, J. Catal. 74 (1982) 77–83, https://doi.org/10.1016/0021-9517(82)90010-0.

[13] M. Aizawa, Y. Morikawa, Y. Namai, H. Morikawa, Y. Iwasawa, Oxygen Vacancy Promoting Catalytic Dehydration of Formic Acid on TiO $_2$ (110) by in Situ Scanning Tunneling Microscopic Observation, J. Phys. Chem. B. 109 (2005) 18831–18838, https://doi.org/10.1021/jp0523773.

[14] H. Onishi, T. Aruga, Y. Iwasawa, Catalytic reactions on a metal oxide single crystal: switchover of the reaction paths in formic acid decomposition on titanium dioxide $TiO_2$(110), J. Am. Chem. Soc. 115 (1993) 10460–10461, https://doi.org/10.1021/ja00075a112.

[15] M.A. Henderson, Complexity in the Decomposition of Formic Acid on the $TiO_2$(110) Surface, J. Phys. Chem. B. 101 (1997) 221–229, https://doi.org/10.1021/jp961494i.

[16] K. Kim, M. Barteau, Pathways for carboxylic acid decomposition on titania, Langmuir 4 (1988) 945–953, https://doi.org/10.1021/la00082a028.

[17] U. Diebold, The surface science of titanium dioxide, Surf. Sci. Rep. 48 (2003) 53–229, https://doi.org/10.1016/S0167-5729(02)00100-0.

[18] K. Fukui, H. Onishi, Y. Iwasawa, Imaging of individual formate ions adsorbed on $TiO_2$(110) surface by non-contact atomic force microscopy, Chem. Phys. Lett. 280 (1997) 296–301, https://doi.org/10.1016/S0009-2614(97)01143-3.

[19] P. Käckell, K. Terakura, Dissociative adsorption of formic acid and diffusion of formate on the $TiO_2$(110) surface: the role of hydrogen, Surf. Sci. 461 (2000) 191–198, https://doi.org/10.1016/S0039-6028(00)00576-8.

[20] S.P. Bates, G. Kresse, M.J. Gillan, The adsorption and dissociation of ROH molecules on $TiO_2$(110), Surf. Sci. 409 (1998) 336–349, https://doi.org/10.1016/S0039-6028(98)00278-7.

[21] A. Vittadini, A. Selloni, F.P. Rotzinger, M. Grätzel, Formic Acid Adsorption on Dry and Hydrated $TiO_2$ Anatase (101) Surfaces by DFT Calculations, J. Phys. Chem. B. 104 (2000) 1300–1306, https://doi.org/10.1021/jp993583b.

[22] K.L. Miller, J.L. Falconer, J.W. Medlin, Effect of water on the adsorbed structure of formic acid on $TiO_2$ anatase (101), J. Catal. 278 (2011) 321–328, https://doi.org/10.1016/j.jcat.2010.12.019.

[23] G.Y. Popova, T.V. Andrushkevich, Y.A. Chesalov, E.S. Stoyanov, In situ FTIR study of the adsorption of formaldehyde, formic acid, and methyl formiate at the surface of $TiO_2$ (anatase), Kinet. Catal. 41 (2000) 805–811, https://doi.org/10.1023/A:1026681321584.

[24] Y. Morikawa, I. Takahashi, M. Aizawa, Y. Namai, T. Sasaki, Y. Iwasawa, First-principles theoretical study and scanning tunneling microscopic observation of dehydration process of formic acid on a $TiO_2$(110) surface, J. Phys. Chem. B. 108 (2004) 14446–14451, https://doi.org/10.1021/jp0497460.

[25] D.H. Kim, M.A. Anderson, Photoelectrocatalytic Degradation of Formic Acid Using a Porous $TiO_2$ Thin-Film Electrode, Environ. Sci. Technol. 28 (1994) 479–483, https://doi.org/10.1021/es00052a021.

[26] S. Wang, E. Iglesia, Experimental and theoretical assessment of the mechanism and site requirements for ketonization of carboxylic acids on oxides, J. Catal. 345 (2017) 183–206, https://doi.org/10.1016/j.jcat.2016.11.006.

[27] S. Brunauer, P.H. Emmett, E. Teller, Adsorption of gases in multimolecular layers, J. Am. Chem. Soc. 60 (1938) 309–319, https://doi.org/10.1021/ja01269a023.

[28] D.R. Stull, Vapor Pressure of Pure Substances. Organic and Inorganic Compounds, Ind. Eng. Chem. 39 (2005) 517–540, https://doi.org/10.1021/ie50448a022.

[29] O.C. Bridgeman, E.W. Aldrich, Vapor pressure tables for water, J. Heat Transfer. 86 (2012) 279, https://doi.org/10.1115/1.3687121.

[30] G. Kresse, J. Hafner, Ab initio molecular-dynamics simulation of the liquid-metal–amorphous-semiconductor transition in germanium, Phys. Rev. B. 49 (1994) 14251–14269, https://doi.org/10.1103/PhysRevB.49.14251.

[31] Furthmüller Kresse, Efficient iterative schemes for ab initio total-energy calculations using a plane-wave basis set, Phys. Rev. B. Condens. Matter. 54 (1996) 11169–11186, https://doi.org/10.1103/physrevb.54.11169.

[32] G. Kresse, J. Furthmüller, Efficiency of ab-initio total energy calculations for metals and semiconductors using a plane-wave basis set, Comput. Mater. Sci. 6 (1996) 15–50, https://doi.org/10.1016/0927-0256(96)00008-0.

[33] J.P. Perdew, K. Burke, M. Ernzerhof, Generalized gradient approximation made simple, Phys. Rev. Lett. 77 (1996) 3865–3868, https://doi.org/10.1103/PhysRevLett. 77.3865.

[34] P.E. Blöchl, Projector augmented-wave method, Phys. Rev. B. 50 (1994) 17953–17979.

[35] S. Grimme, Semiempirical GGA-type density functional constructed with a long-range dispersion correction, J. Comput. Chem. 27 (2006) 1787–1799, https://doi.org/10.1002/jcc.

[36] M. Lazzeri, A. Vittadini, A. Selloni, Structure and energetics of stoichiometric $TiO_2$ anatase surfaces, Phys. Rev. B. 63 (2001) 1–9, https://doi.org/10.1103/PhysRevB.63.155409.

[37] G. Mills, H. Jónsson, G.K. Schenter, Reversible work transition state theory: application to dissociative adsorption of hydrogen, Surf. Sci. 324 (1995) 305–337, https://doi.org/10.1016/0039-6028(94)00731-4.

[38] G. Henkelman, H. Jónsson, A dimer method for finding saddle points on high dimensional potential surfaces using only first derivatives, J. Chem. Phys. 111 (1999) 7010–7022, https://doi.org/10.1063/1.480097.

[39] Donald A. McQuarrie, Statistical Mechanics, University Science Books, Sausalito, CA, 2000.

[40] P. Deshlahra, E. Iglesia, Methanol Oxidative Dehydrogenation on Oxide Catalysts: Molecular and Dissociative Routes and Hydrogen Addition Energies as Descriptors of Reactivity, J. Phys. Chem. C. 118 (2014) 26115–26129, https://doi.org/10.1021/jp507922u.

[41] C.T. Campbell, J.R.V. Sellers, Enthalpies and entropies of adsorption on well-De fi ned Oxide Surfaces: experimental measurements, Chem. Rev. 113 (2013) 4106–4135, https://doi.org/10.1021/cr300329s.

[42] K.L. Miller, C.W. Lee, J.L. Falconer, J.W. Medlin, Effect of water on formic acid photocatalytic decomposition on $TiO_2$and Pt/$TiO_2$, J. Catal. 275 (2010) 294–299, https://doi.org/10.1016/j.jcat.2010.08.011.

[43] A. Zecchina, S. Bordiga, G. Spoto, D. Scarano, G. Spanò, F. Geobaldo, IR spectroscopy of neutral and ionic hydrogen-bonded complexes formed upon interaction of $CH_3OH$, $C_2H_5OH$, $(CH_3)_2O$, $(C_2H_5)_2O$ and $C_4H_8O$ with H-Y, H-ZSM-5 and H-mordenite: comparison with analogous adducts formed on the H-Nafion superacidi, J. Chem. Soc., Faraday Trans. 92 (1996) 4863–4875, https://doi.org/10.1039/FT9969204863.

[44] K. Fukuda, Y. Noto, T. Onishi, K. Tamaru, Mechanism of dehydration decomposition of formic acid over alumina and silica. Adsorption measurements during the catalytic reaction, Trans. Faraday Soc. 63 (1967) 3072, https://doi.org/10.1039/tf9676303072.

[45] S. Wang, K. Goulas, E. Iglesia, Condensation and esterification reactions of alkanals, alkanones, and alkanols on $TiO_2$: Elementary steps, site requirements, and synergistic effects of bifunctional strategies, J. Catal. 340 (2016) 302–320, https://doi.org/10.1016/j.jcat.2016.05.026.

[46] J. Strunk, W.C. Vining, A.T. Bell, A study of oxygen vacancy formation and annihilation in submonolayer coverages of $TiO_2$ dispersed on MCM-48, J. Phys. Chem. C. 114 (2010) 16937–16945, https://doi.org/10.1021/jp100104d.

[47] H. Liu, H. Ma, X. Li, W. Li, M. Wu, X. Bao, The enhancement of $TiO_2$ photocatalytic activity by hydrogen thermal treatment, Chemosphere 50 (2003) 39–46, https://doi.org/10.1016/S0045-6535(02)00486-1.

[48] J. Towns, T. Cockerill, M. Dahan, I. Foster, K. Gaither, A. Grimshaw, et al., XSEDE: accelerating scientific discovery, Comput. Sci. Eng. 16 (2014) 62–74, https://doi.org/10.1109/MCSE.2014.80.